SMC-TR-98-24

AEROSPACE REPORT NO.
TR-98(1055)-1

Space Environment Test of Materials for Inflatable Structures

16 April 1998

Prepared by

W. K. STUCKEY, M. J. MESHISHNEK,
W. D. HANNA, and F. D. ROSS
Mechanics and Materials Technology Center
Technology Operations

Prepared for

SPACE AND MISSILE SYSTEMS CENTER
AIR FORCE MATERIEL COMMAND
2430 E. El Segundo Boulevard
Los Angeles Air Force Base, CA 90245

Space Systems Group

THE AEROSPACE CORPORATION
El Segundo, California

This report was submitted by The Aerospace Corporation, El Segundo, CA 90245-4691, under Contract No. F04701-93-C-0094 with the Space and Missile Systems Center, 2430 E. El Segundo Blvd., Los Angeles Air Force Base, CA 90245. It was reviewed and approved for The Aerospace Corporation by S. Feuerstein, Principal Director, Mechanics and Materials Technology Center.

This report has been reviewed by the Public Affairs Office (PAS) and is releasable to the National Technical Information Service (NTIS). At NTIS, it will be available to the general public, including foreign nationals.

This technical report has been reviewed and is approved for publication. Publication of this report does not constitute Air Force approval of the report's findings or conclusions. It is published only for the exchange and stimulation of ideas.

Lt. J. Bishop, USAF
AFRL/VSDV

REPORT DOCUMENTATION PAGE

Form Approved
OMB No. 0704-0188

1. AGENCY USE ONLY (*Leave blank*)	2. REPORT DATE	3. REPORT TYPE AND DATES COVERED
	16 April 1998	

4. TITLE AND SUBTITLE

Space Environment Test of Materials for Inflatable Structures

5. FUNDING NUMBERS

F04701-93-C-0094

6. AUTHOR(S)

W. K. Stuckey, M. J. Meshishnek, W. D. Hanna, and F. D. Ross

7. PERFORMING ORGANIZATION NAME(S) AND ADDRESS(ES)

The Aerospace Corporation
Technology Operations
El Segundo, CA 90245-4691

8. PERFORMING ORGANIZATION REPORT NUMBER

TR-98(1055)-1

9. SPONSORING/MONITORING AGENCY NAME(S) AND ADDRESS(ES)

Space and Missile Systems Center
Air Force Materiel Command
2430 E. El Segundo Boulevard
Los Angeles Air Force Base, CA 90245

10. SPONSORING/MONITORING AGENCY REPORT NUMBER

SMC-TR-98-24

11. SUPPLEMENTARY NOTES

12a. DISTRIBUTION/AVAILABILITY STATEMENT

Approved for public release; distribution unlimited

12b. DISTRIBUTION CODE

13. ABSTRACT (*Maximum 200 words*)

Materials being considered for use in thin-film applications of inflatable structures were exposed to a simulated space environment representing a 5-year Low Earth Orbit (LEO) and also to a 5-year Geo-synchronous Orbit (GEO). Solar absorptance and tensile test measurements were performed, pre- and posttest. The materials consisted of various thin polymer foils, including 0.0005-in. bare and metal-lized Kapton E, LaRC-CP1, LaRC-CP2, FEP Teflon, Triton conductive COR, and slightly thicker (0.0008 to 0.0018-in.) films of Triton TOR, Triton TOR-LM, and Triton TOR-RC. A total of 34 sam-ples were exposed plus control and contamination monitors.

Measurements of solar absorptance and tensile properties were made on samples corresponding to both Low Earth and Geosynchronous Orbit exposures. Increases in solar absorptance were observed for many of the samples. Changes in mechanical properties are also indicated by the results, but there was scatter in the test data due to the limitation of the number of samples that allowed only two of each type to be exposed to each orbital condition, and some to only GEO exposure conditions.

The property changes on thin polymer films due to space environmental exposure must be considered in the design of inflatable structures. The Kapton E samples and the fluorinated polyimides (CP1 and CP2) showed the least degradation. The low-modulus version of TOR (TOR-LM) appeared to be the most stable of the other films.

14. SUBJECT TERMS

Materials, Space environmental effect, Polymer films, Inflatable structures

15. NUMBER OF PAGES

35

16. PRICE CODE

17. SECURITY CLASSIFICATION OF REPORT	18. SECURITY CLASSIFICATION OF THIS PAGE	19. SECURITY CLASSIFICATION OF ABSTRACT	20. LIMITATION OF ABSTRACT
UNCLASSIFIED	UNCLASSIFIED	UNCLASSIFIED	

NSN 7540-01-280-5500

Standard Form 298 (Rev. 2-89)
Prescribed by ANSI Std. Z39-18
298-102

Acknowledgements

The authors wish to acknowledge L'Garde, Inc., Tustin, California, SRS Technologies, Huntsville, Alabama, and Triton Systems, Inc., Chelmsford, MA., for the contribution of the samples for this investigation.

Contents

Figures

Tables

1. Introduction

Inflatable antennas are being developed for use in space to take advantage of the potential for lower packaging volumes and lighter weights. These antennas would consist of thin polymer membranes for forming the antenna reflector surface and more robust inflatable, then rigidizable, structural elements to support the antenna. The Large Inflatable Structure Program has the objective of building a large inflatable on-axis reflector. The design of the inflatable lenticular structure that forms the reflector antenna includes a transparent canopy film and a second, metallized reflector film. The current material being considered for these components is 0.5 mil Kapton E. While Kapton E is a newer version of a well-characterized material, Kapton, very little, if any, data exist on the space environmental stability of this newer version. For space applications, it must be shown that the design can tolerate the orbital environment, which includes the effects of solar radiation and electron/proton radiation on the mechanical response on the materials, as well as atomic oxygen erosion for the possible LEO applications. The highest radiation concern is with the thin-film canopy and reflector materials, although all antenna materials need to be capable of tolerating the orbital environment and maintaining properties within the mission requirements.

A test of the candidate thin-film materials for inflatable antenna structures has been performed in the Space Environmental Effects Chamber in the Mechanics and Materials Technology Center of Technology Operations at The Aerospace Corporation. This chamber provides a solar ultraviolet, electron, and proton simulation of the space environment, although the protons were not used for this test. Solar absorptance was measured on samples of each material before the test began. Each sample was cut from a larger sheet of the polymer film which was, in turn, used to prepare the actual test specimens.

The first portion of the test exposed the samples to an environment corresponding to five years at a LEO orbit of 480 nmi and an inclination of 57°. Samples were removed for LEO solar absorptance end-of-life measurements and retained for mechanical testing. The exposure then continued to 5-year GEO conditions (19270 nmi) for the remaining samples. Solar absorptance at end-of-life for the GEO samples was then measured. The mechanical properties of all exposed and control samples were measured at the conclusion of the test. Samples were stored in a dry nitrogen-purged container prior to mechanical testing.

2. Experimental

The Space Environmental Effects Chamber (Figure 1) used to provide the simulation of the LEO and GEO space environment contains a 2500 W Xenon arc lamp for long-wavelength ultraviolet (UV) (230–400 nm) and a 150 W deuterium arc lamp for vacuum ultraviolet (VUV) radiation (115–200 nm). Beam sizes are a nominal 10 in. x 12 in. for long wavelength UV and 7 in. x 7 in. for VUV. The UV beams have a uniformity within 50% but contain small central hot spots. The electron beam is more uniform at about 10%. The beam energy is variable from 5 kV to 120 kV, with flux roughly proportional to electron energy and a function of beam spot size (max. 1000 cm^2). All beams are confocal. The chamber is turbopumped and cryopumped, and the base pressure is currently 2 x 10^{-9} torr. The volume is roughly 400 liters, with a sample table (12 in. x 48 in.) capable of temperature control from –150°C to +150°C, but kept at about 25°C for these tests. Computerized data acquisition is used for chamber diagnostics, which include several temperature and electron flux measurements.

For this study, degradation of the light sources has not been estimated. Rather, the deuterium lamp is assumed to have no degradation over the relatively short number of real-time exposure hours. The Xenon light source is periodically refocused upwards to maintain a near-constant reading on the solar cell. Minor variations across the sample table have also been ignored since the major factor in sample degradation is assumed to be due to the electron exposure.

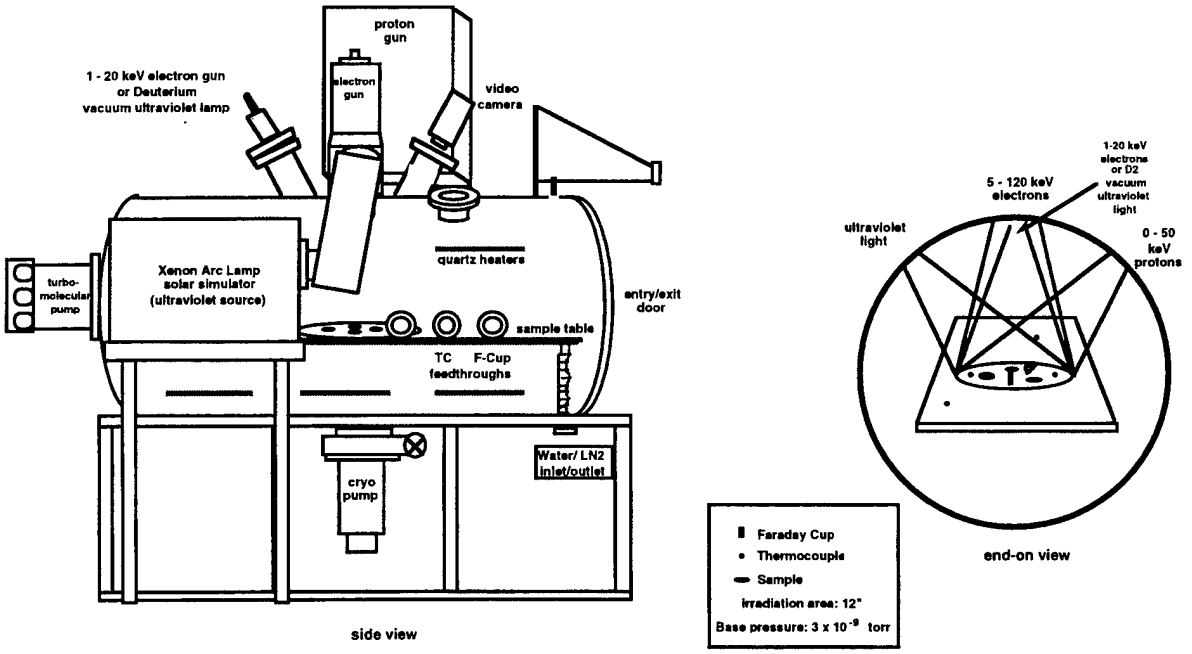

Figure 1. The space environmental effects chamber.

Table 1 lists the materials included in the test. Samples were provided to The Aerospace Corporation by the companies indicated. All samples were 0.5 mil except for some of the Triton materials since 0.5 mil samples of some of their materials were not available for this test. Machine direction or transverse direction was not maintained, but all samples were cut in parallel strips from one sheet of polymer film. In order to accommodate the maximum number of samples, 1-in.-wide samples with lengths of 4 to 6 in. were wrapped around a 1 in. x 2 in. x 0.060 in. copper plate and taped on the back with small pieces of 3M adhesive-backed Kapton tape, with the polymer side facing out. The exposed area on the front was then used for solar property measurements and was also the test area between the grips when the mechanical properties were determined using an Instron Universal Testing Instrument. With this size sample, it was possible to include 34 samples. The sample arrangement in the chamber for the test is shown in Figure 2. The larger area represents the approximately 10 in. x 12 in. area covered by the Xenon lamp. The area covered by the deuterium lamp is about 7 in. in diameter, so it illuminates most, but not all, samples. The solar cell is used as a diagnostic during the exposure to monitor the Xenon lamp output. The Faraday cups monitor the electron flux at several locations during the electron exposure. An Optical Solar Reflector (OSR) is present as a check for any contamination that might condense during the test and potentially affect test results. No contamination was detected during this test as evidenced by the very small changes (0.001) in the reflectance of the OSR.

An inflatable antenna used on an orbiting satellite may or may not be continuously in full sun. About 5000 sun-hours is typical for a 5-year mission for a spacecraft surface exposure, with degradation greatest in the early exposure times. Material properties normally have stabilized with a 5000 equivalent sun-hour exposure. The electrons were added in the presence of Solar UV in the final stages of each exposure. The UV was not started until the chamber pressure was in the low to mid 10^{-8} torr region. After accumulation of 2657 equivalent UV sun-hours (1080 h, at a solar intensity of 2.46 suns), the electron doses shown in Table 2 were added to correspond to a LEO orbit of 480 nmi at a 57° inclination. These fluences are based on predicting the electron depth-dose profile in Kapton for the assumed orbit using AE8 predictions of electron fluences, and then choosing the best set of reasonable conditions using the set energies of the electron gun on the chamber to match the depth-dose profile via a linear combination of multiple energies. For the thin 0.5-mil materials, the orbital

Table 1. Radiation Test Matrix

Simulation Samples	Sample Designator	Provider	Number of Samples	LEO/GEO
Kapton E	E	L'Garde	4	LEO & GEO
Kapton E/650 A° Ag/90 A° Inconel 600	EAG	L'Garde	4	LEO & GEO
Kapton E/650 A° Au/50 A° Cr/500 A° Al	EAU	L'Garde	4	LEO & GEO
Butt Joint Seam	BJS	L'Garde	2	LEO & GEO
CP1	CP1	SRS Technologies	4	LEO & GEO
CP2	CP2	SRS Technologies	4	LEO & GEO
TOR/1200A° Ag/300A° Inconel	TOR	Triton Systems, Inc.	2	GEO Only
TOR-RC/1200A° Ag/300A° Inconel	RC	Triton Systems, Inc.	2	GEO Only
TOR-LM	LM	Triton Systems, Inc.	4	LEO & GEO
Conductive COR/1200A° Ag/300A° Inconel	COR	Triton Systems, Inc.	2	GEO Only
FEP Teflon	FEP	L'Garde	2	LEO & GEO
Total number of samples			34	

dose profile (in representative Kapton) is well matched using only three energies—10, 20 and 40 kV. For the thicker Triton materials, it is necessary to use four energies incorporating 100 kV electrons for further penetration into the polymers. For this reason, 100 kV electrons were also used for the GEO exposure. The prediction curves are shown in Figure 3 for Low Earth Orbit Exposure and Figure 4 for Geosynchronous Orbit. The electron exposures were performed starting with the highest energy first and progressing successively to lower energies.

Table 2. Predicted Electron Fluence for Simulation

Low Earth Orbit Exposure

Energy (kV)	Fluence, electrons/cm^2	Exposure Time, hours @6.25e8/s
10	1.9e13	8
20	2.0e13	9
40	4.3e13	19

Geosynchronous Orbit Exposure

Energy (kV)	Fluence, electrons/cm^2	Exposure Time, hours @6.25e9/s
10	5.5e14	24
20	8.0e14	36
40	8.3e14	37
100	3.0e15	133

Predictions are ±10%.

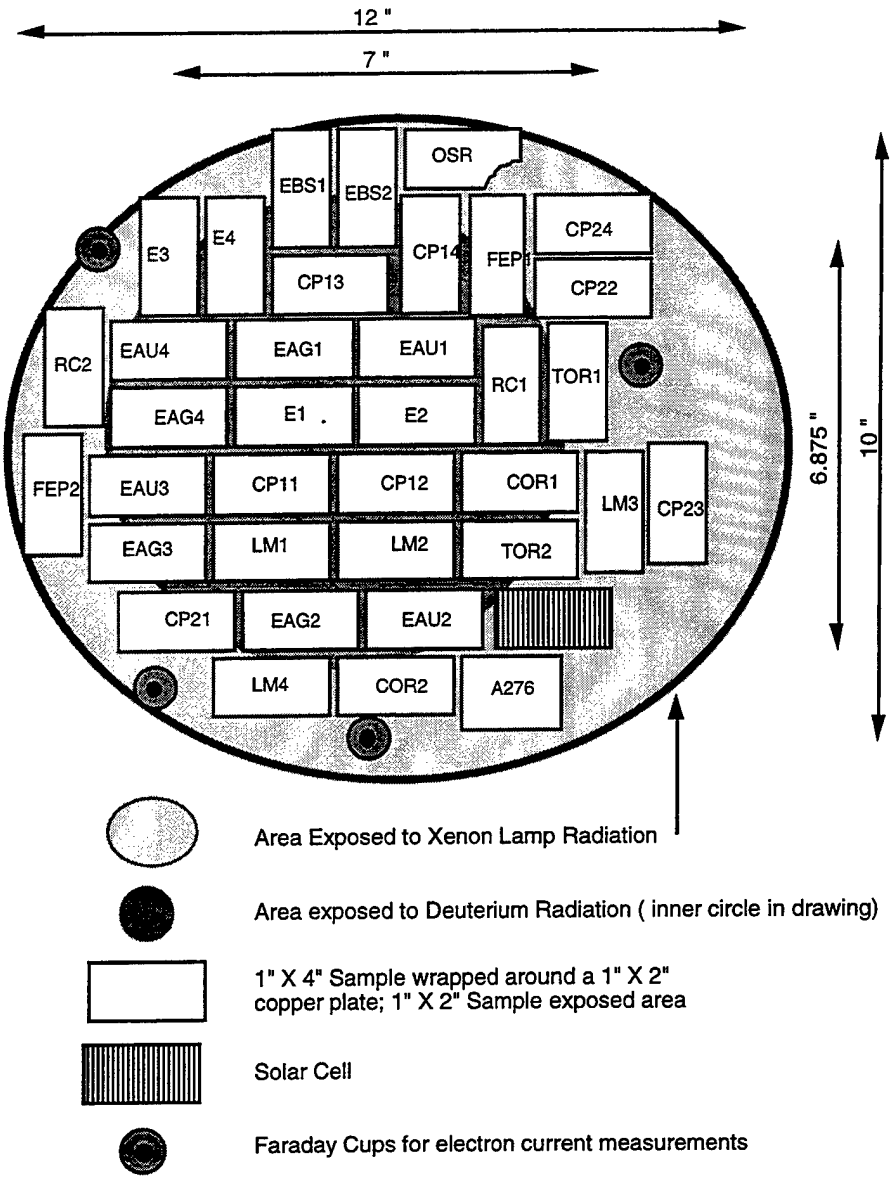

Figure 2. Test configuration for inflatable materials samples.

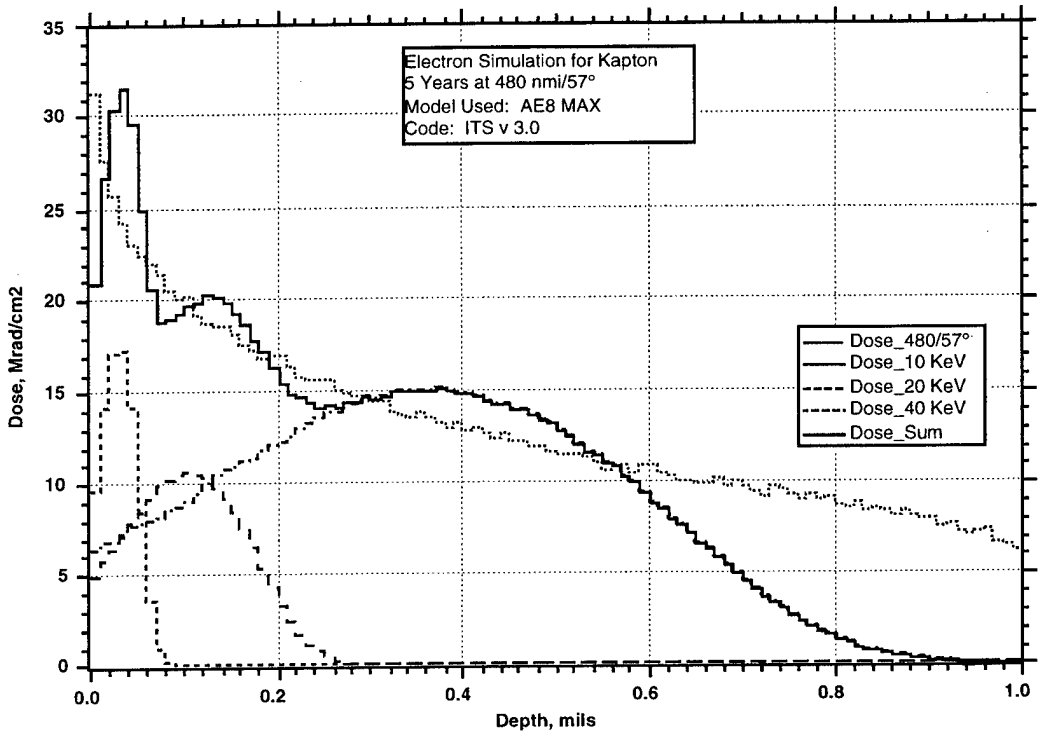

Figure 3. Predicted simulation dose profiles and orbital dose profile for 480 nmi/57° LEO orbit.

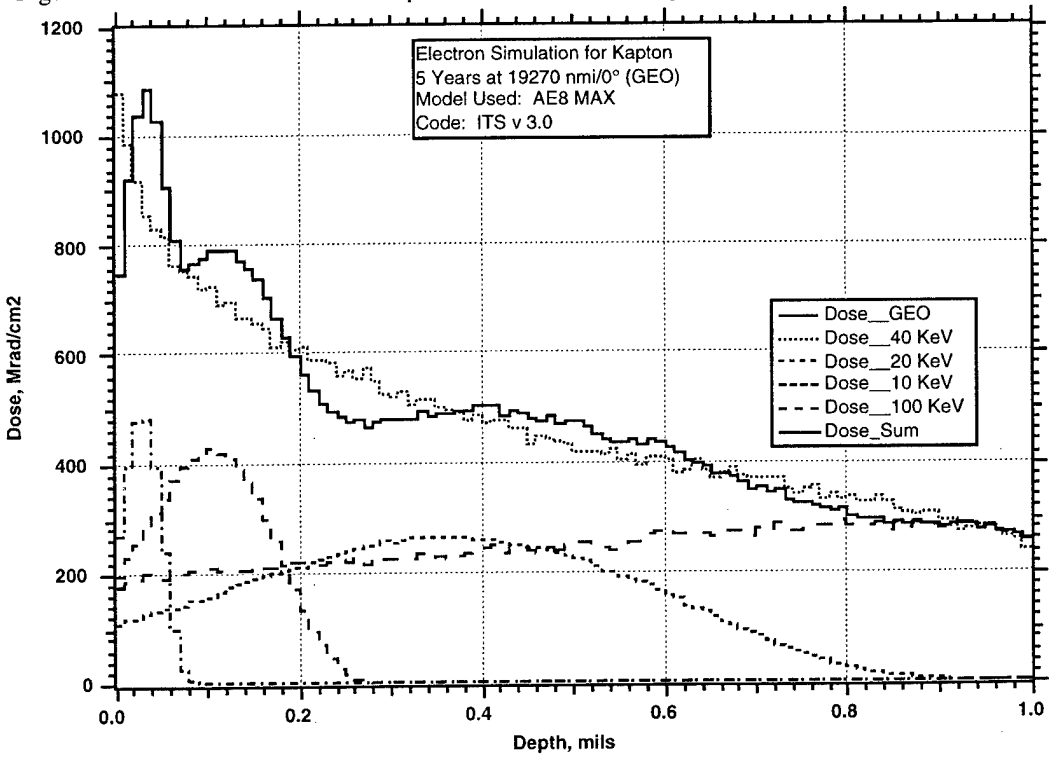

Figure 4. Predicted simulation dose profiles and orbital dose profile for GEO orbit.

After 3200 equivalent UV sun-hours, (1301 h, at a solar intensity of 2.46 suns), the LEO electron exposure was completed, and the samples were removed for analysis and measurements. The UV exposure was then continued on the remaining samples up to 4430 h (1801 h, at a solar intensity of 2.46 suns), while the GEO electron dose was added. Throughout the entire exposure, the deuterium lamp was cycled on periodically (effectively 3.5 h/day) to accumulate approximately the same number of equivalent UV sun-hours as the xenon source. The deuterium source has been estimated to have an initial output of about 17 solar constants over its operating wavelength range, as compared to about 2.5 for the xenon source.

After exposure to the LEO or GEO radiation levels the specimens were removed from the copper mounting plate and stored in a dry-nitrogen environment until they were tested; however, the solar absorptance was measured as soon as possible after removal from the chamber.

The Ultraviolet-Visible-Near Infrared (UV-VIS-NIR) diffuse hemispherical reflectance was measured on a Perkin-Elmer Lambda-9 equipped with a 6-in. Labsphere, Inc. Spectralon-coated integrating sphere. The reflectance measurements were made using a 240 nm/min scan rate, 2-nm slit width, 0.5-s response, with the scan range being 250–2500 nm. The reflectance spectrum was background-corrected and referenced to a NIST 2019d White Tile Diffuse Reflectance Standard. This procedure references the sample spectrum to a NIST perfect diffuser rather than the Spectralon integrating sphere coating. Correction factors are calculated and applied to the sample spectrum from the measured NIST Standard. The accuracy of the reflectance measurements is ±2%. A trapezoidal approximation to the two integrals that define the ASTM Solar Air Mass Zero curve and the measured reflectance spectrum is then calculated. The calculation involves 137 points corresponding to the 137 wavelength bins that define the ASTM Solar Air Mass Zero curve from 250 to 2500 nm. The calculation of the solar absorptance makes use of the Kirchoff relationship, which states that any energy (or in this case light) that is not reflected or transmitted, must be absorbed. Therefore, the solar absorptance (α) can be calculated from the hemispherical reflectance (ρ) and diffuse transmittance (τ) by the equation: $\alpha = 1 - \rho - \tau$. If the material is opaque, then the transmittance, τ, is zero, and, therefore, $\alpha = 1 - \rho$. For transmissive materials (all nonmetallized), the diffuse transmittance was also measured using the same instrumentation; however, there is no correction applied to the sample spectrum beyond the background correction of the machine.

For mechanical testing, the specimens were removed from the dry box one at a time and laid on a template to mark the extent of the gauge length and to assure that the gauge length coincided with the exposed area of the specimen. After marking, each specimen was placed in 10-lb pinch grips fitted with hard rubber faces. The upper grip was attached to a 50-lb load cell, and the lower grip was attached to the lower platen of the model 1127 Instron Universal Testing Instrument. The testing was conducted at a crosshead rate of 0.02 in/min, which is equivalent to a strain rate of 1% per minute. Load and displacement data were recorded on the Instron strip chart recorder and simultaneously on a PC fitted with a 12-bit A-to-D converter. Specimen strains were calculated from crosshead position because the specimens were not substantial enough to support a contact type of extensometer, and the only non-contact type of extensometer available depends upon a stable surface reflection, which was not present in these specimens.

3. Results

During the exposure, photographs were taken periodically through the chamber viewports, and a short video was taken through an overhead viewport each day. Representative photos of the samples taken during the exposure are shown in Figures 5–8. Refer to Figure 2 to identify each sample. Very soon after the start of the solar UV exposure, an apparent cloudiness developed in the FEP Teflon samples. No significant changes were noted in the other samples through the LEO exposure. When the electron radiation was resumed to continue exposure to GEO conditions, the COR2 sample was observed to crack nearly completely at one edge where it was folded around the copper substrate. When it was removed after the GEO exposure, it broke into small fragments and could not be used for any posttest measurements. The COR1 sample also broke upon removal from the chamber but had a fragment large enough for a solar absorptance measurement. It could not be mechanically tested. TOR2 also broke at the edge of the sample when an attempt was made to remove the TOR2 from the copper substrate. The FEP Teflon samples lost their cloudiness upon removal from the chamber. The LEO-exposed sample was tested and showed degradation that was not unexpected. FEP Teflon is known to degrade at radiation exposures in the 10-krad range. The FEP Teflon sample exposed to GEO conditions could not be removed from the copper substrate. A reflectance measurement of the Teflon on the copper was made, but there was not a good copper reference spectrum to allow spectral subtraction to obtain useful data. It appears that the cloudiness was associated with contact with the substrate, and did not appear to be any permanent visible change in the FEP Teflon. The CP1 and CP2 samples showed slight color variations (light brown) as indicated by the solar absorptance measurements. The Kapton E samples were not visibly altered at any time during the test.

The results of the solar absorptance measurements are shown for all samples in the Appendix. Table 3 is the average of the samples of each type included in the test, even though some samples were in the deuterium beam while others were not. Some samples were metallized and others were not, but they are easily distinguished by the higher reflectance for the metallized samples and zero transmittance. The significant data is the change in solar absorptance that occurred for each material. The Kapton E showed little change in solar absorptance, and in the cases of the metallized Kapton E samples, displayed slight increases in reflectance (lower absorptance). The CP-1 and CP-2 samples showed small increases in solar absorptance. The data for the TOR-LM and TOR-RC samples show modest increases in solar absorptance. The values for the TOR and COR samples were measured immediately after completion of the test and are considered to be valid although the fragility of the samples made handling and potential damage during handling a concern in the measurements.

Generally, the metallized samples tended to show increases in reflectance posttest. The notable exceptions are COR and TOR-RC. Inspection of the layout and the data for "identical" samples in which one was in the deuterium beam, and one was not, show little difference in solar absorptance changes. Exceptions to this are TOR-LM and TOR-RC; however, the effects observed are opposite in these two cases. Scatter in the data due to small numbers of samples of each type prevent firm conclusions from being drawn. However, it seems apparent that the Kapton E materials are quite stable. This data is in marked contrast to that reported for aluminized Kapton (presumably Kapton H) from

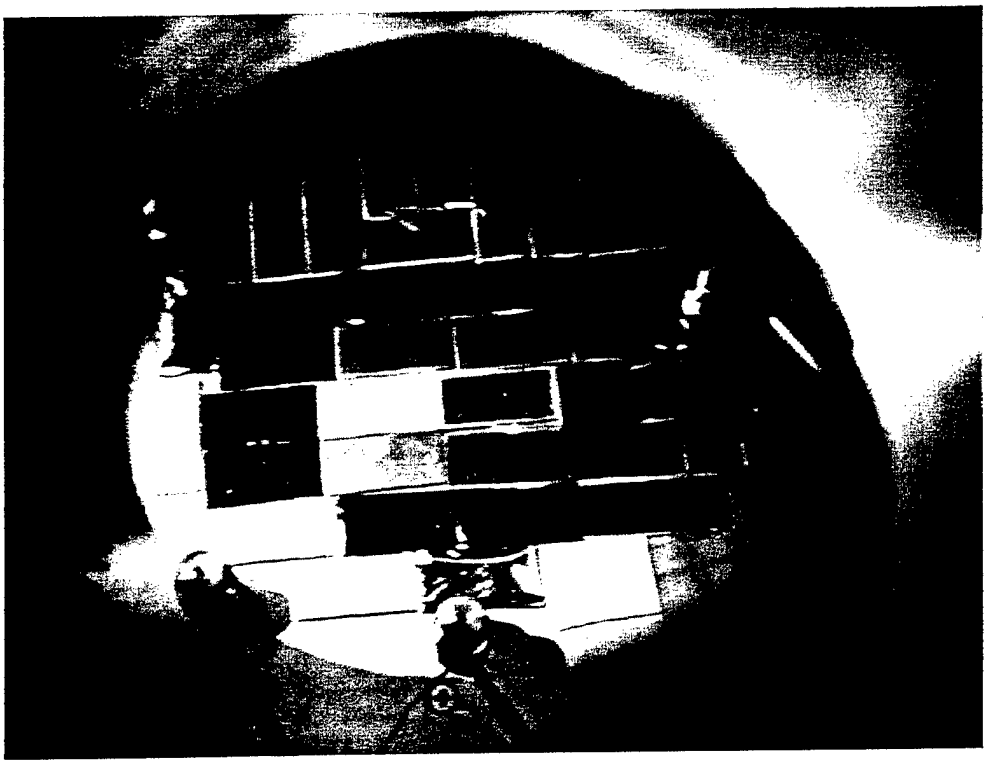

Figure 5. Photograph of samples at beginning of test.

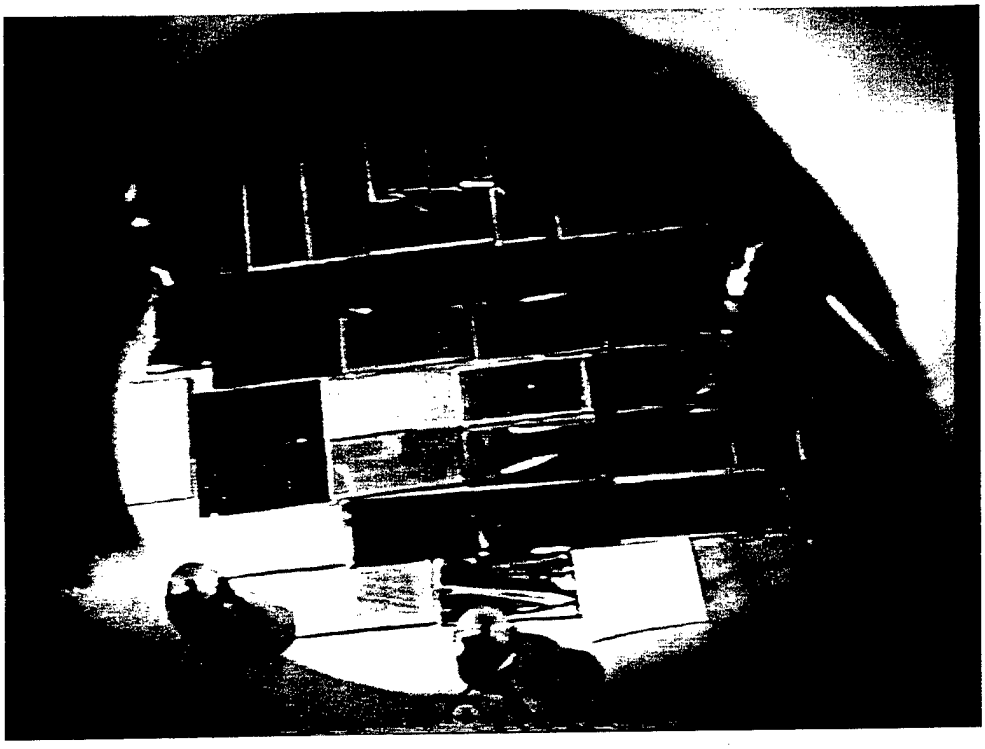

Figure 6. Photograph of samples at end of LEO Exposure.

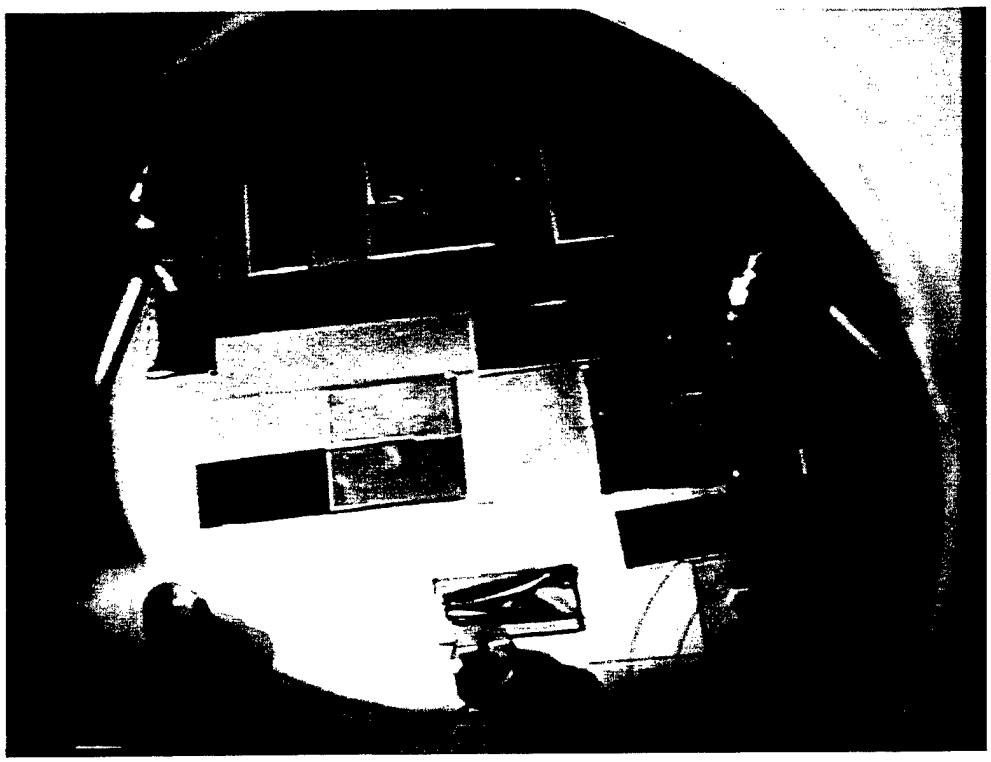

Figure 7. Photograph of samples near end of GEO Exposure.

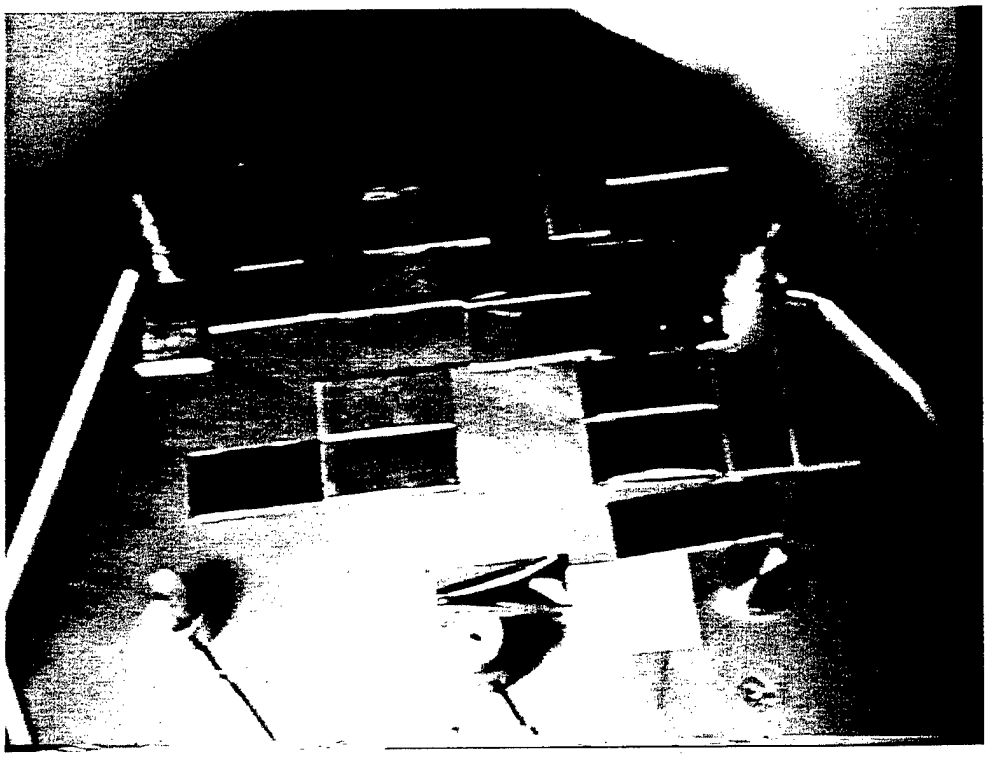

Figure 8. Photograph of samples at end of test.

Table 3. Summary of Solar Absorptance Measurements

Material	Thickness (mil)	Reflectance			Transmittance			Absorptance		
		Pre-test	LEO Post-test	GEO Post-test	Pre-test	LEO Post-test	GEO Post-test	Pre-test	LEO Post-test	GEO Post-test
Kapton E	0.5	0.136	0.144	0.147	0.683	0.679	0.674	0.181	0.176	0.189
Kapton E/650 A° Ag/90 A° Inconel 600	0.5	0.752	0.766	0.773	0.000	0	0	0.248	0.234	0.227
Kapton E/650 A° Au/50 A° Cr/500 A° Al	0.5	0.535	0.550	0.542	0.000	0	0	0.465	0.450	0.458
CP1	0.5	0.094	0.100	0.098	0.830	0.796	0.745	0.076	0.103	0.154
CP2	0.5	0.100	0.097	0.103	0.834	0.809	0.805	0.066	0.092	0.090
FEP Teflon	0.5	0.048	0.055	**	0.955	0.945	**	-0.003	0	**
Conductive COR/1200A° Ag/300A° Inconel	0.9	0.608		0.532	0.000		0	0.392		0.468
TOR/1200A° Ag/300A° Inconel	0.9	0.684		0.710	0.000		0	0.316		0.290
TOR-LM	0.9	0.110	0.114	0.712	0.776	0.722	0.705	0.114	0.164	0.193
TOR-RC/1200A° Ag/300A° Inconel	2.0	0.813		0.712	0.000		0	0.187		0.288

** Sample could not be measured

the SCATHA experiment. For a five-year SCATHA exposure, one expects about a 0.14 increase in solar absorptance.[1] The value of 0.57 obtained for Aeroglaze A-276 end-of-test solar absorptance compares well with the values seen on LDEF.[2] However, since the radiation environment on LDEF was quite low, one would expect a higher value for the solar absorptance here. At the end of the LEO exposure, the A-276 sample measured 0.44 for solar absorptance. This lower-than-expected value may be due to complex rate effects not reproducible in the time allowed for the tests. Reflectance and transmittance curves for selected samples are included in the Appendix.

The results of the tensile tests are summarized in Table 4 from an average of the measured results for each material (see Appendix). Because the tensile tests were performed without the benefit of an

Table 4. Summary of Apparent Modulus Measurements

Material	Thickness (mil)	Pre-test (ksi)	LEO Post-test (ksi)	GEO Post-test (ksi)
Kapton E	0.5	555	670	595
Kapton E/650 A° Ag/90 A° Inconel 600	0.5	575	455	630
Kapton E/650 A° Au/50 A° Cr/500 A° Al	0.5	630	695	605
CP1	0.5	335	270	345
CP2	0.5	360	305	365
FEP Teflon	0.5	55	35	**
Conductive COR/1200A° Ag/300A° Inconel	0.9	450		**
TOR/1200A° Ag/300A° Inconel	0.9	298		130
TOR-LM	0.9	220	170	210
TOR-RC/1200A° Ag/300A° Inconel	2.0	240		200

** Sample could not be measured

extensometer to measure displacements, the strain values presented should be considered as a close approximation, rather than an absolute representation, of the actual behavior. Thus, the slope of the initial portion of each stress-strain curve is designated as the "apparent modulus" rather than "elastic modulus." It can be seen that there is considerable variation in these values, even among the control samples. For example, of the five control samples tested for the gold-coated Kapton E (see Appendix), the apparent modulus varied between 510 and 710 ksi, resulting in an error of approximately ±15%. This is likely the result of slight differences in the gauge length of samples and perhaps variations in tightening of the grips on the test fixtures. However, since each sample was tested in an identical fashion, comparisons between samples and conditions can be considered valid. As mentioned above, samples that were "identical," but in different UV/VUV exposure areas, generally did not show appreciable differences in mechanical properties within the range of experimental error.

In spite of the scatter in the mechanical test results, there are some observations that can be made. There was no significant degradation in the properties of Kapton E or the CP1 and CP2 samples, although one CP1 and one CP2 sample exposed to LEO showed lower mechanical response. The FEP Teflon exposed to GEO exposure and the Conductive COR samples degraded sufficiently that no measurements were possible. The TOR sample and the TOR-RC sample also apparently degraded from the radiation exposures. The TOR-LM showed little change in three of the four samples tested, although one of the LEO exposed samples did show lower mechanical response.

Each sample was tested until failure even though that was not the prime range of interest for this test. There is also quite a bit of variation in the failure stress and failure strain of individual samples, again, even among the control samples. This can occur because of minor nicks or roughness of cut edges during sample preparation, which can lead to premature failure, either in the gauge length or at the edge of the grip. Thus, failure stresses and strains should, in themselves, be viewed with caution as indicators of comparative behavior. This issue is usually resolved by the use of replicate samples, which were limited in this study. The failure location of each specimen was noted and is recorded in the table in the Appendix. The full stress-strain curves were obtained, up to failure, and are available for most samples in the Appendix. The initial portion of the stress-strain curves for three selected samples are shown in Figures 9–11.

For an inflatable antenna, the reflector side of the lenticular structure would be metallized to provide a reflective surface. The resistance of metallized samples of Kapton E after the LEO and GEO exposure conditions was measured at L'Garde using a four-point probe with a span of about 1 in. Data are shown in Table 5. Unexposed resistance data for each type of sample was obtained from eight measurements on unexposed samples. For each sample in the test, measurements were made at three locations. Each sample was about 6 in. long, which allowed measurements to be made in the center portion that was exposed during the test and the two ends of the sample that were not exposed (two to four measurements at each location). The data from the ends of the sample are shown in the unexposed column, and the data from the center portion is shown in the LEO Exposure and GEO exposure columns. The resistance of the silver sample may have changed slightly for the LEO exposure but has apparently decreased by more than 10% for the GEO exposure. The gold-coated samples show appreciable increases for the LEO and GEO exposures. It is an interesting observation, but the mechanism for these changes is not known.

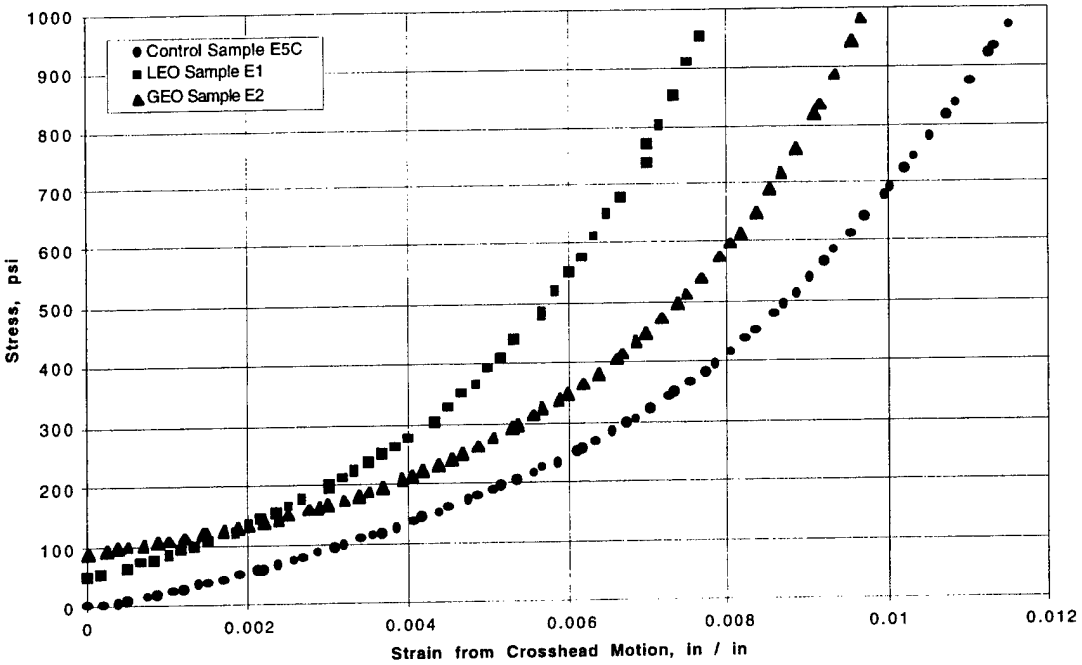

Figure 9. Stress-strain curves for initial loading of 0.0005 inch uncoated Kapton E foil.

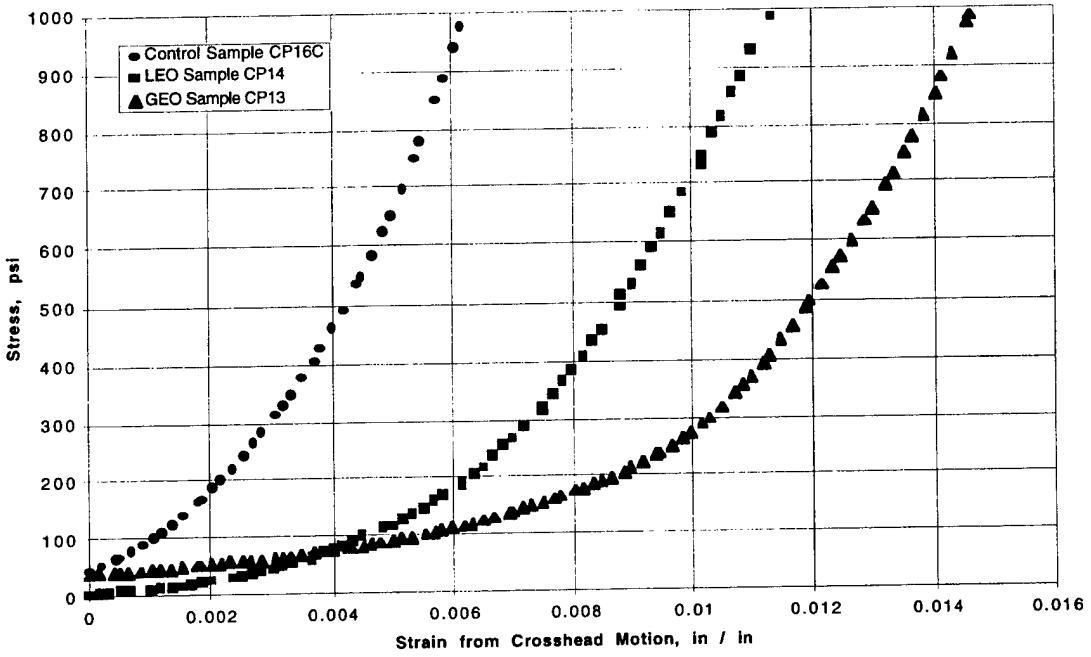

Figure 10. Stress-strain curves for initial loading of 0.0005 inch LaRC-CP1 foil.

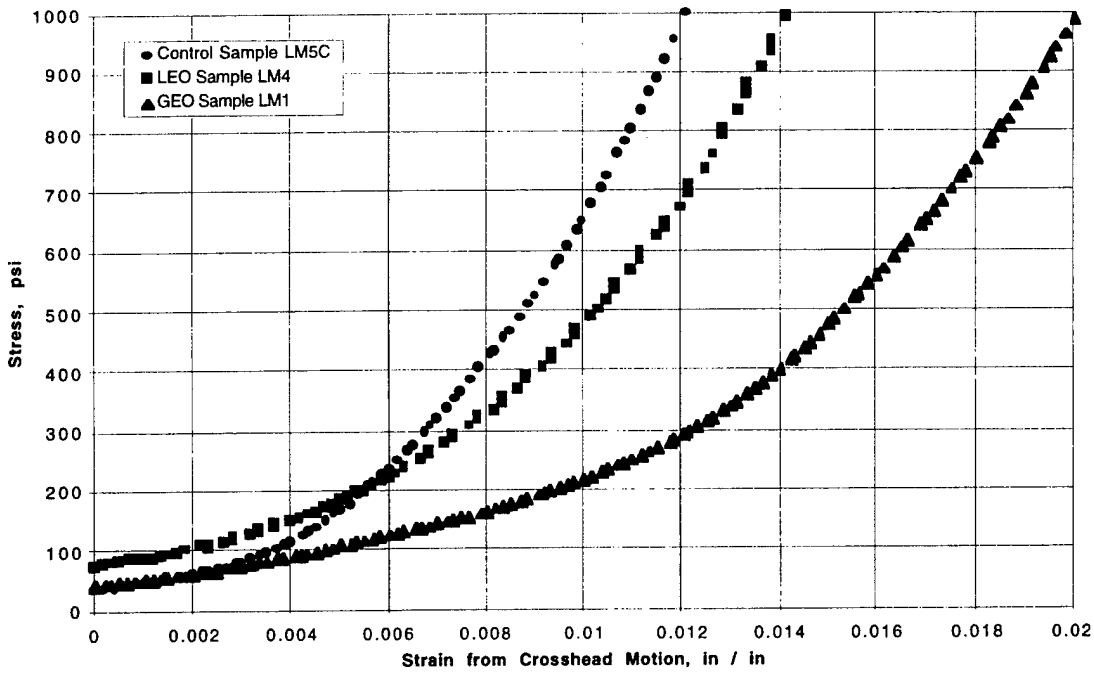

Figure 11. Stress-strain curves for initial loading of 0.0008 inch Triton TOR-LM foil.

Table 5. Effect of LEO and GEO Exposure on Resistance of Metallized Kapton E.

	Resistance (ohms)		
Sample	**Unexposed**	**LEO Exposure**	**GEO Exposure**
Kapton E/650 A° Ag/90 A° Inconel 600	0.581 ± 0.016		
EAG2	0.607 ± 0.002	0.562 ± 0.000	
EAG4	0.557 ± 0.013	0.570 ± 0.009	
EAG1	0.571 ± 0.059		0.503 ± 0.000
EAG3	0.570 ± 0.027		0.500 ± 0.000
Kapton E/650 A° Au/50 A° Cr/500 A° Al	1.314 ± 0.057		
EAU2	1.269 ± 0.027	1.535 ± 0.025	
EAU3	1.242 ± 0.053	2.306 ± 0.091	
EAU1	1.367 ± 0.068		2.070 ± 0.150
EAU4	1.601 ± 0.369		3.228 ± 0.018

4. Summary

The typical application using these films would be designed to work in the range below 1000 psi. However, it is very difficult to obtain reliable and reproducible data in this range. The apparent modulus reported here is for the region where the stress-strain curve becomes linear, which is typically above the range between 100 and 2,000 psi. In this test, we were looking for evidence of degradation in the properties of the film and not attempting to obtain design properties. The data for the initial loading up to 1000 psi are shown in Figures 9, 10, and 11 for selected samples of Kapton E, CP2, and TOR-LM. For the fluorinated polyimide and TOR-LM samples, it would appear that the strain at an intermediate stress level of 500 psi appears to increase with a LEO exposure and further with a GEO exposure for the same mission duration, five years in these tests. That is, with a given design stress, the yield of the polymer would increase with the orbital environment, and the effect is greater with GEO orbits than with LEO orbits. The Kapton E data is scattered. Any conclusion based on this limited data set is not reasonable except that changes in mechanical properties were found. These effects need to be better defined but would need to be taken into account during the lifetime on orbit. Similarly, the changes in solar absorptance would need to be included to account for space environment effects.

Additional testing of some of these materials with larger numbers of samples of fewer materials would be prudent to obtain data with higher confidence levels and less scatter. TOR-LM, Kapton E, and CP2 are viable candidates for further experiments based on these results.

A test of a variety of potential materials for inflatable structures that use thin polymer films has been completed. Measurements of solar absorptance and tensile properties were made on samples corresponding to both Low Earth and Geosynchronous Orbits. The Kapton E samples and the fluorinated polyimides showed the least degradation. The low modulus version of TOR from Triton Systems, Inc., appeared to be the most stable of the Triton films. It would appear from the GEO data that the reflectance of the metallized TOR is stable, and, therefore, at lower dose levels the polymer might be mechanically stable, thus allowing TOR to be used in LEO applications.

References

1. D. F. Hall and A. A. Fote, "Thermal Control Coatings Performance at Near Geosynchronous Altitude," *J. Thermophys. Heat Transfer* **6**, 665–671 (1992).

2. J. L. Golden, "Results of Examination of the A276 White and Z306 Black Thermal Control Paint Disks Flown on LDEF," *LDEF—69 Months in Space First Post-Retrieval Symposium*, NASA Conference Publication 3134 975–987 (1991).

Appendix

List of Samples (Table 1A)

Pre- and Posttest Solar Absorptance Results (Table 2A)

Selected Reflectance and Transmittance Curves (Figs. 1A–12A)

Tensile Test Results (Table 3A)

Selected Stress-Strain Curves (Figs. 13A–20A)

Table 1A. List of Samples

Sample ID	Description	LEO/GEO
E1	Kapton E	LEO
E2	Kapton E	GEO
E3	Kapton E	GEO
E4	Kapton E	LEO
EAG1	Kapton E/650 A° Ag/90 A° Inconel 600	GEO
EAG2	Kapton E/650 A° Ag/90 A° Inconel 600	LEO
EAG3	Kapton E/650 A° Ag/90 A° Inconel 600	GEO
EAG4	Kapton E/650 A° Ag/90 A° Inconel 600	LEO
EAU1	Kapton E/650 A° Au/50 A° Cr/500 A° Al	GEO
EAU2	Kapton E/650 A° Au/50 A° Cr/500 A° Al	LEO
EAU3	Kapton E/650 A° Au/50 A° Cr/500 A° Al	LEO
EAU4	Kapton E/650 A° Au/50 A° Cr/500 A° Al	GEO
EBS1	Butt Joint Seam	GEO
EBS2	Butt Joint Seam	LEO
CP11	CP1	GEO
CP12	CP1	LEO
CP13	CP1	GEO
CP14	CP1	LEO
CP21	CP2	LEO
CP22	CP2	LEO
CP23	CP2	GEO
CP24	CP2	GEO
FEP1	FEP Teflon	GEO
FEP2	FEP Teflon	LEO
TOR1	Triton TOR	GEO
TOR2	Triton TOR	GEO
LM1	Triton TOR-LM	GEO
LM2	Triton TOR-LM	LEO
LM3	Triton TOR-LM	GEO
LM4	Triton TOR-LM	LEO
RC1	Triton TOR-RC	GEO
RC2	Triton TOR-RC	GEO
COR1	Triton Conductive COR	GEO
COR2	Triton Conductive COR	GEO
A276	Aeroglaze A276 white paint	GEO
OSR	OCLI Optical Solar Reflector	GEO

Table 2A. Pre- and Post-test Solar Absorptances

Sample ID	Exposure	Solar Reflectivity		Solar Transmissivity		Solar Absorptance	
		Pre-test	Post-test	Pre-test	Post-test	Pre-test	Post-test
E1	LEO	0.136	0.148	0.683	0.679	0.181	0.173
E2	GEO	0.136	0.144	0.683	0.673	0.181	0.183
E3	GEO	0.136	0.149	0.683	0.676	0.181	0.175
E4	LEO	0.136	0.139	0.683	0.679	0.181	0.182
EAG1	GEO	0.752	0.776	0	0	0.248	0.224
EAG2	LEO	0.752	0.759	0	0	0.248	0.241
EAG3	GEO	0.752	0.770	0	0	0.248	0.230
EAG4	LEO	0.752	0.773	0	0	0.248	0.227
EAU1	GEO	0.535	0.557	0	0	0.465	0.443
EAU2	LEO	0.535	0.553	0	0	0.465	0.447
EAU3	LEO	0.535	0.546	0	0	0.465	0.454
EAU4	GEO	0.535	0.526	0	0	0.465	0.474
FEP1	GEO	0.048	*	0.955	*	-0.003	*
FEP2	LEO	0.048	0.055	0.955	0.945	-0.003	0
CP11	GEO	0.094	0.096	0.830	0.733	0.076	0.171
CP12	LEO	0.094	0.100	0.830	0.790	0.076	0.11
CP13	GEO	0.094	0.100	0.830	0.762	0.076	0.138
CP14	LEO	0.094	0.100	0.830	0.803	0.076	0.097
CP21	LEO	0.100	0.103	0.834	0.801	0.066	0.096
CP22	LEO	0.100	0.092	0.834	0.819	0.066	0.089
CP23	GEO	0.100	0.104	0.834	0.806	0.066	0.09
CP24	GEO	0.100	0.103	0.834	0.808	0.066	0.089
COR1	GEO	0.608	0.532	0	0	0.392	0.468
COR2	GEO	0.608	*	0	*	0.392	*
TOR1	GEO	0.684	0.713	0	0	0.316	0.287
TOR2	GEO	0.684	0.706	0	0	0.316	0.294
LM1	GEO	0.110	0.106	0.776	0.685	0.114	0.209
LM2	LEO	0.110	0.114	0.776	0.717	0.114	0.169
LM3	GEO	0.110	0.108	0.776	0.725	0.114	0.167
LM4	LEO	0.110	0.113	0.776	0.728	0.114	0.159
RC1	GEO	0.813	0.739	0	0	0.187	0.261
RC2	GEO	0.813	0.684	0	0	0.187	0.316
A276	GEO	0.726	0.424	0	0	0.274	0.576
OSR	GEO	0.954	0.953	0	0	0.046	0.047

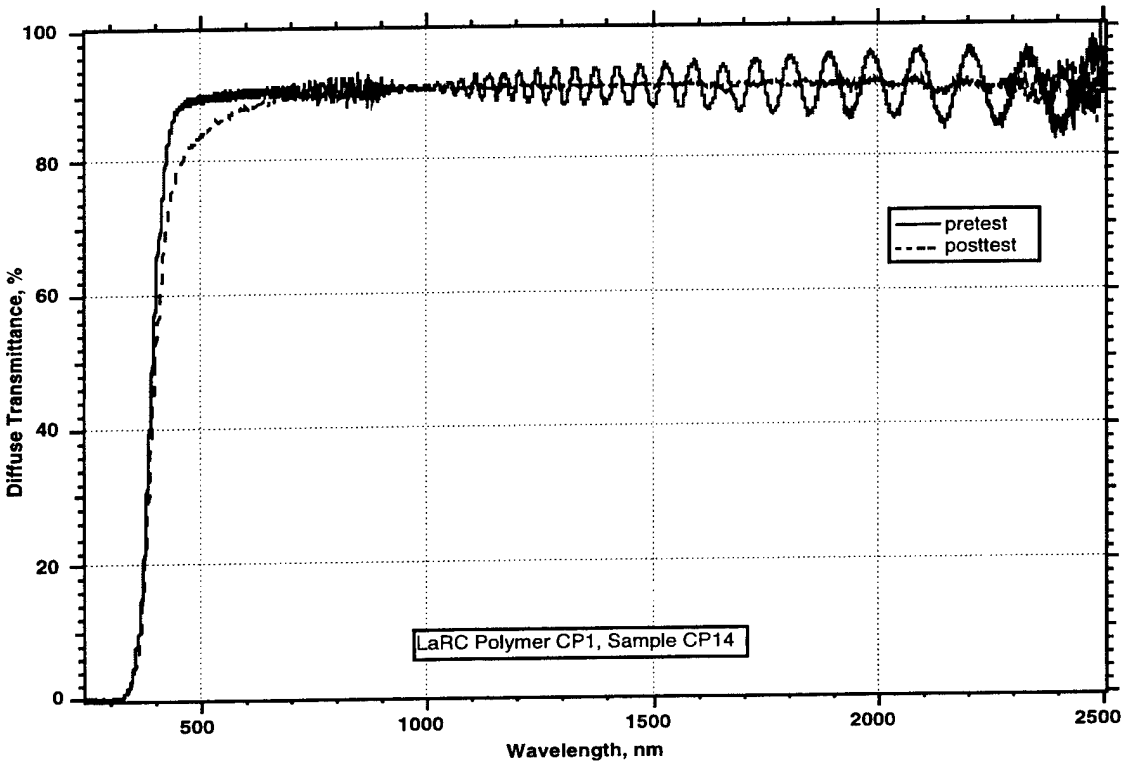

Figure 1A. Transmittance curve for Sample CP14; LEO Exposure.

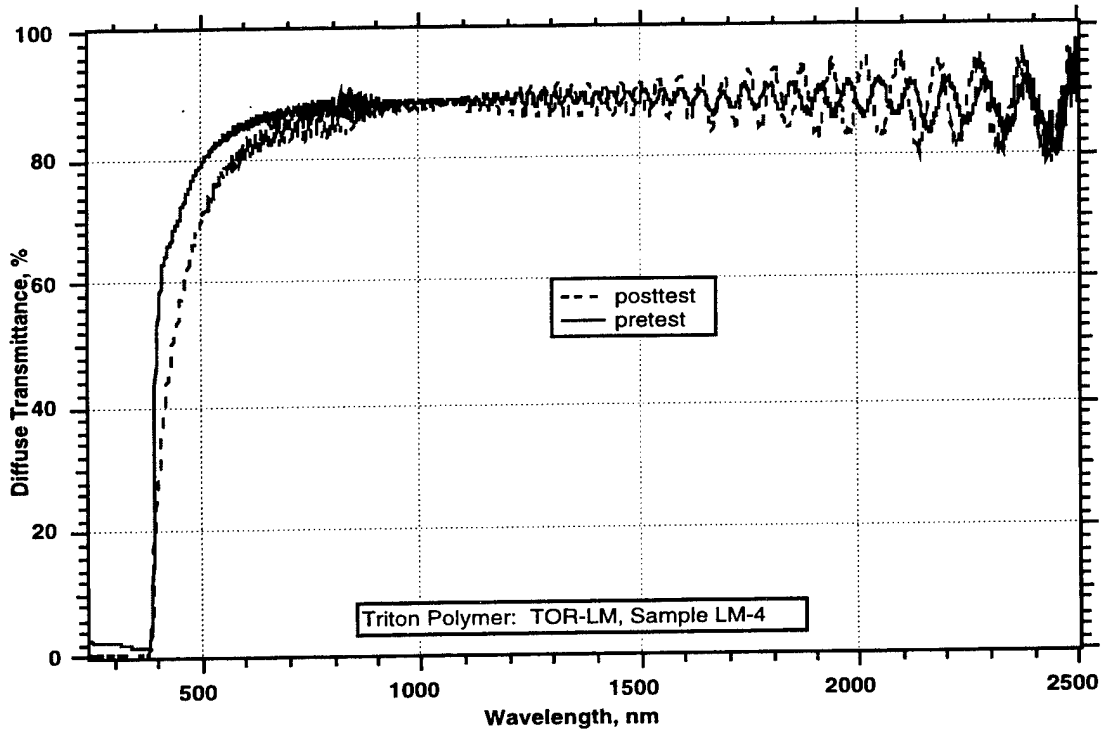

Figure 2A. Transmittance curve for Sample LM-4; LEO Exposure.

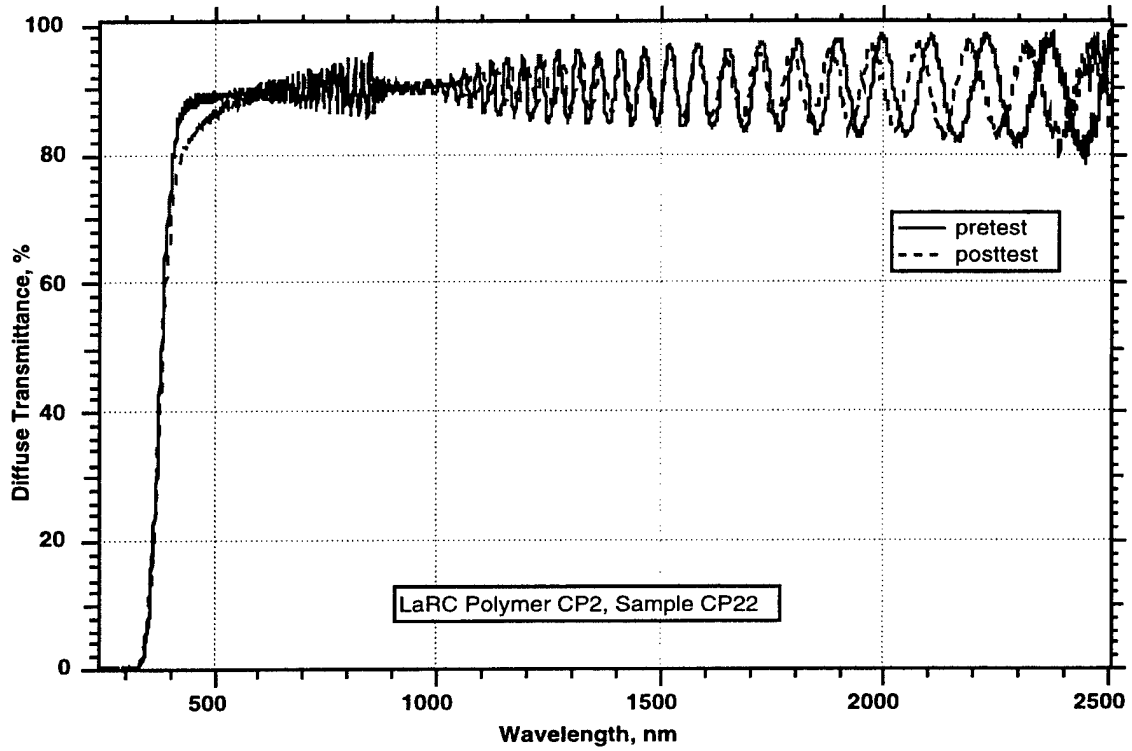

Figure 3A. Transmittance curve for Sample CP22; LEO Exposure.

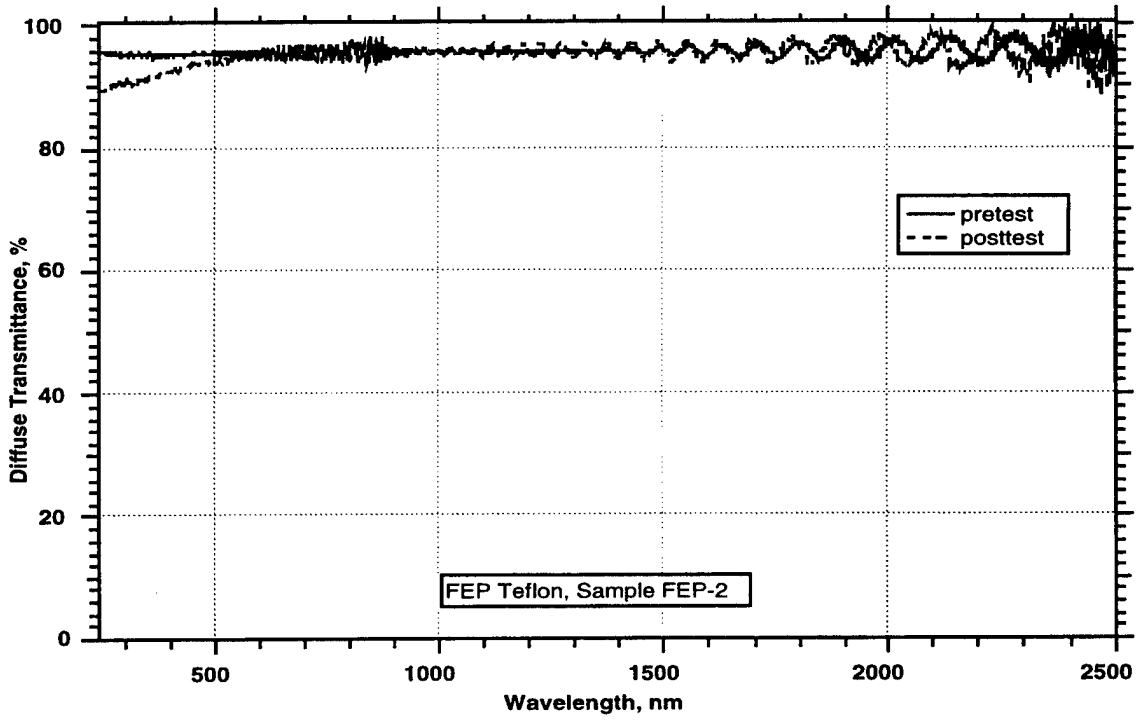

Figure 4A. Transmittance curve for Sample FEP2; LEO Exposure.

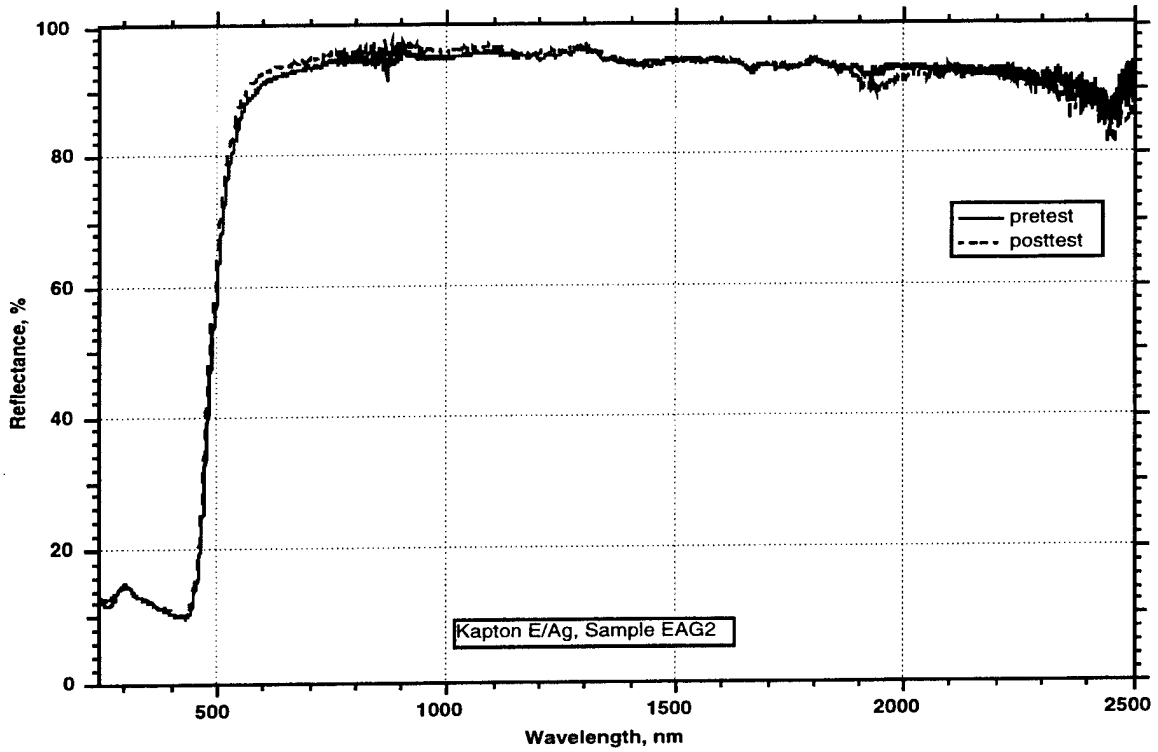

Figure 5A. Reflectance curve for Sample EAG2; LEO Exposure.

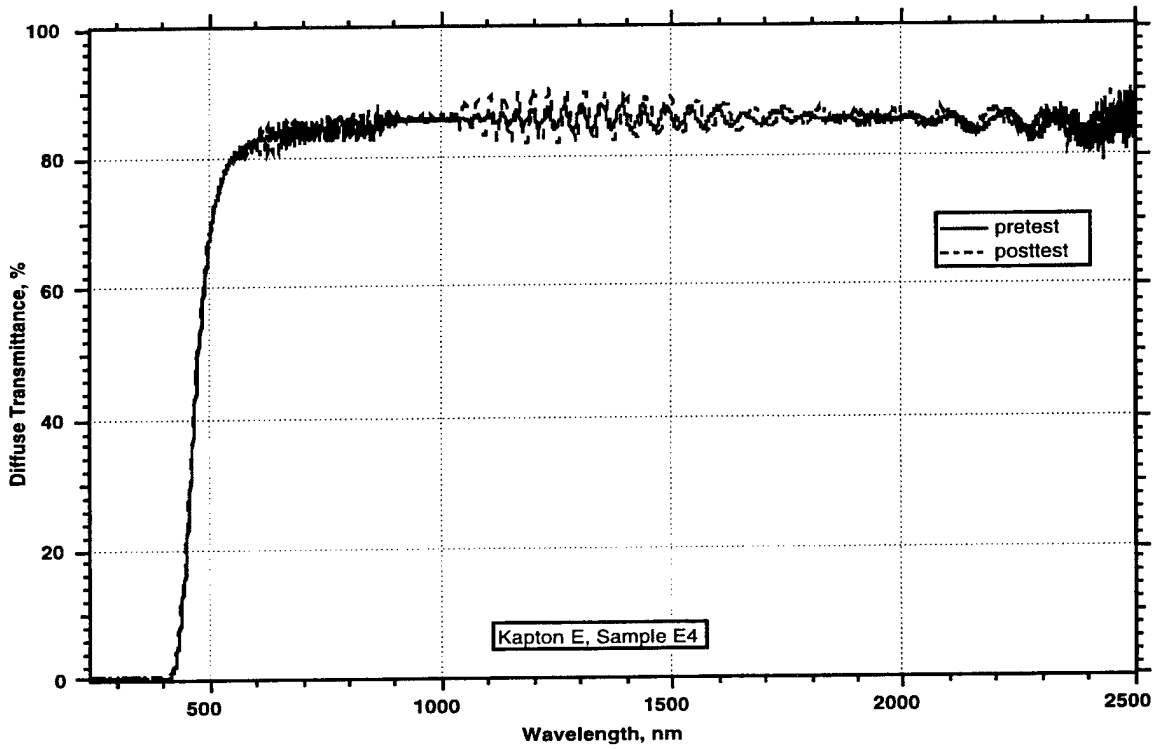

Figure 6A. Transmittance curve for Sample E2; LEO Exposure.

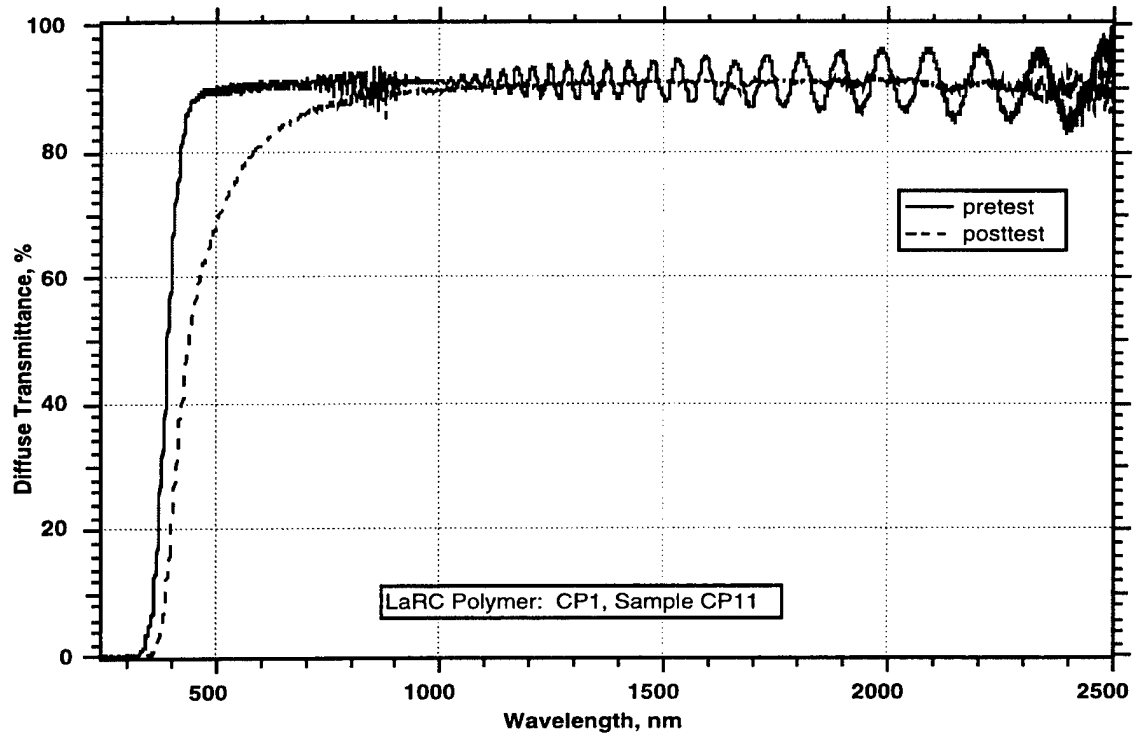

Figure 7A. Transmittance curve for Sample CP11; GEO Exposure.

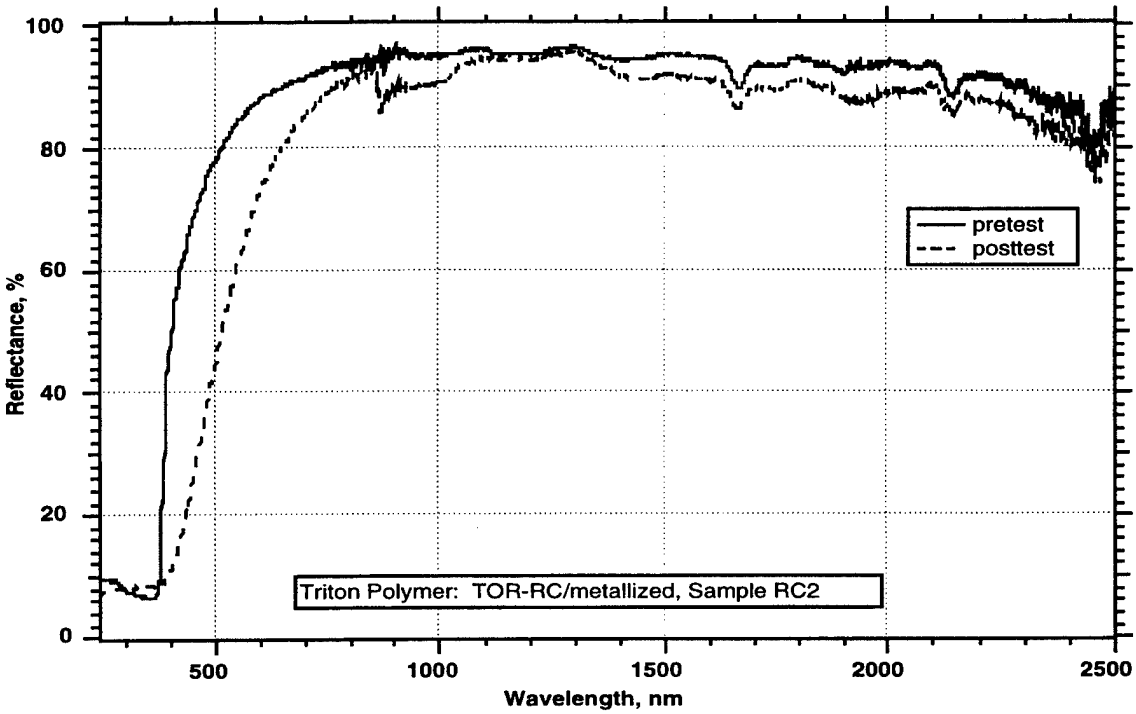

Figure 8A. Reflectance curve for Sample RC2; GEO Exposure.

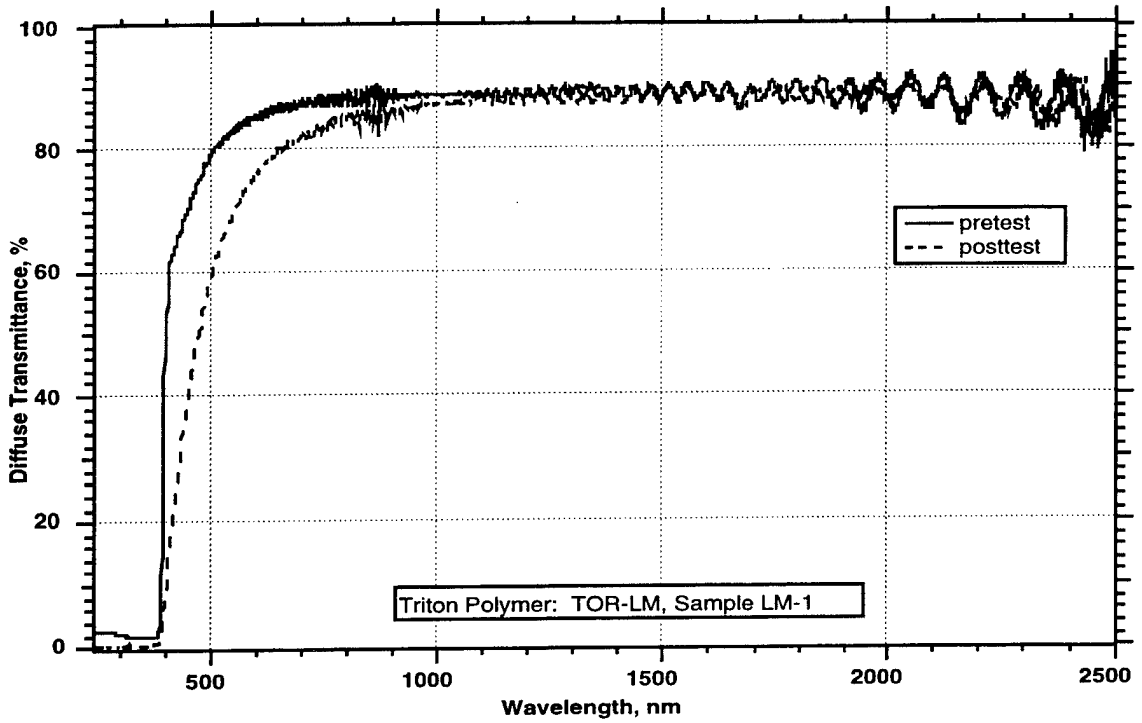

Figure 9A. Transmittance curve for Sample LM-1 GEO Exposure.

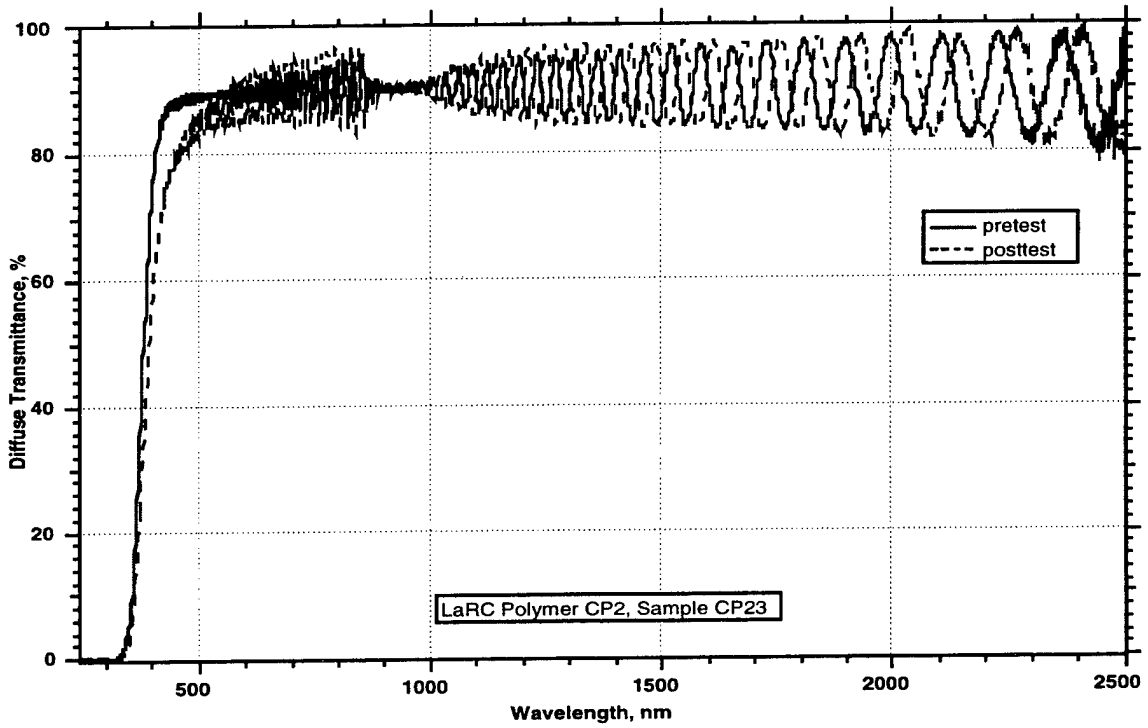

Figure 10A. Transmittance curve for Sample CP23; GEO Exposure.

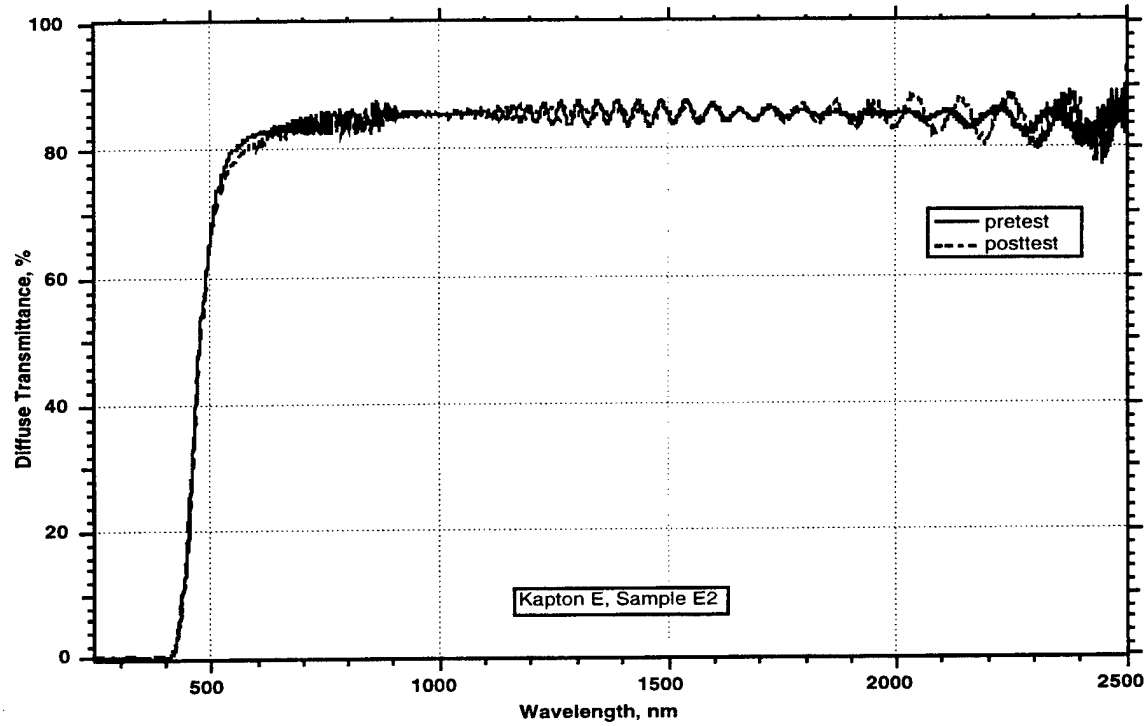

Figure 11A. Transmittance curve for Sample E2; GEO Exposure.

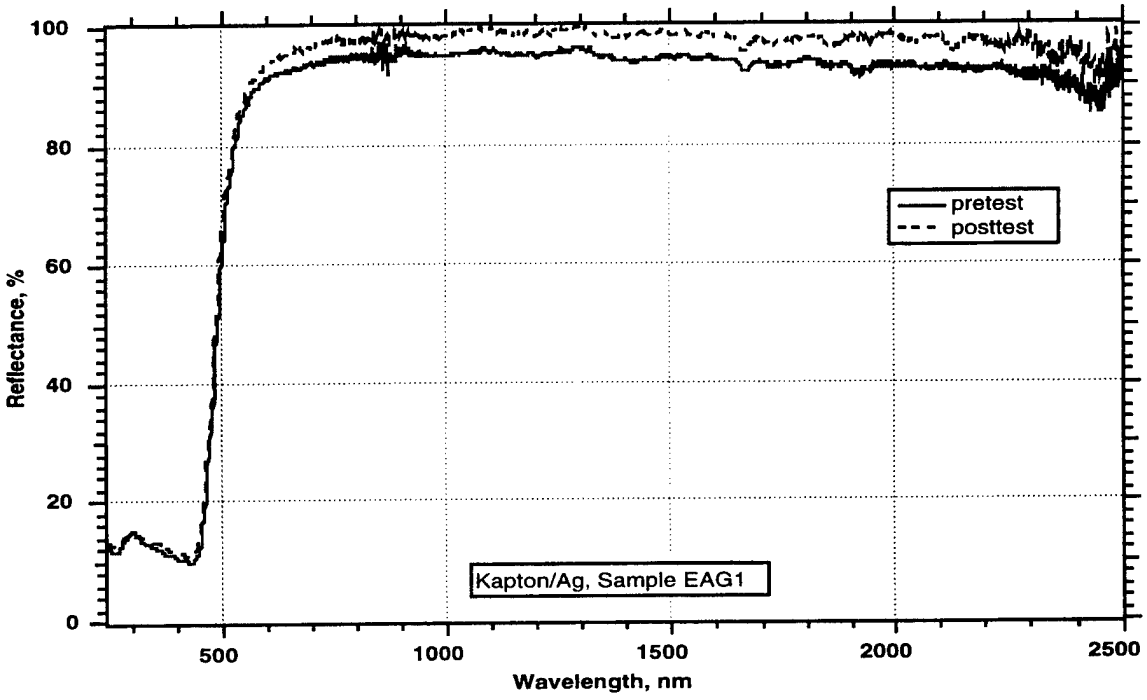

Figure 12A. Transmittance curve for Sample EAG1; GEO Exposure.

Table 3A. Tensile Test Results for Materials for Inflatable Structures

Material Description	Sample ID	Thickness (mil)	Apparent Modulus (ksi)	Failure Stress (ksi)	Apparent Failure Strain (%)	Fracture Description	Sample Description
Kapton E	E5C	0.5	570	43.8	43.0	Gage Area	Control
	E6C	0.5	540	26.1	14.3	Grip Edge	Control
	E1	0.5	690	23.5	5.5	Gage Area	LEO
	E4	0.5	620	20.6	4.7	Grip Edge	LEO
	E2	0.5	600	36.8	23.7	Gage Area	GEO
	E3	0.5	590	19.0	4.1	Gage Area	GEO
Kapton E/650 Å Ag/90 Å Inconel 600	EAG5C	0.5	590	31.7	25.3	Grip Edge	Control
	EAG6C	0.5	560	37.6	47.8	Grip Edge	Control
	EAG2	0.5	590	35.0	35.6	Grip Edge	LEO
	EAG4	0.5	320	18.3	7.4	Grip Edge	LEO
	EAG1	0.5	640	40.2	40.7	Gage Area	GEO
	EAG3	0.5	610	25.3	7.2	Gage Area	GEO
Kapton E/650 Å Au/50 Å Cr/500 Å Al	EAU5C	0.5	610	36.9	45.7	Grip Edge	Control
	EAU6C	0.5	620	23.6	6.3	Gage Area	Control
	EAU7C	0.5	510	29.2	16.7	Gage Area	Control
	EAU8C	0.5	710	38.5	50.5	Gage Area	Control
	EAU9C	0.5	700	41.4	43.1	Grip Edge	Control
	EAU2	0.5	490	33.5	27.2	Grip Edge	LEO
	EAU3	0.5	570	21.3	5.5	Gage Area	LEO
	EAU1	0.5	570	32.1	21.2	Grip Edge	GEO
	EAU4	0.5	640	28.6	10.1	Gage Area	GEO
LaRC-CP1	CP15C	0.5	330	12.2	4.9	Gage Area	Control
	CP16C	0.5	340	15.0	7,4	Gage Area	Control
	CP12	0.5	230	12.8	7.1	Grip Edge	LEO
	CP14	0.5	310	9.8	4.3	Gage Area	LEO
	CP11	0.5	340	11.9	4.6	Gage Area	GEO
	CP13	0.5	350	9.4	3.0	Gage Area	GEO
LaRC-CP2	CP25C	0.5	350	14.5	4.9	Gage Area	Control
	CP26C	0.5	370	12.9	4.4	Gage Area	Control
	CP21	0.5	330	9.7	3.0	Grip Edge	LEO
	CP22	0.5	280	8.6	3.1	Grip Edge	LEO
	CP23	0.5	350	13.0	4.7	Gage Area	GEO
	CP24	0.5	380	13.5	4.6	Grip Edge	GEO
FEP Teflon	FEP3C	0.5	58	3.0	78.9	Grip Edge	Control
	FEP4C	0.5	52	3.1	91.2	Gage Area	Control
	FEP2	0.5	35	2.6	41.2	Gage Area	LEO
	FEP1	0.5	-	-	-	Handling	GEO
Triton TOR-LM	LM5C	0.8	240	7.5	4.1	Grip Edge	Control
	LM6C	0.8	200	7.1	4.1	Gage Area	Control
	LM2	0.8	130	3.1	3.2	Grip Edge	LEO
	LM4	0.8	210	7.3	5.6	Grip Edge	LEO
	LM1	0.8	190	3.3	1.7	Grip Edge	GEO
	LM3	0.8	230	7.9	4.7	Grip Edge	GEO
Triton Conductive COR	COR3C	0.5	420	10.3	2.6	Gage Area	Control
	COR4C	0.5	480	11.6	2.8	Gage Area	Control
	COR1	0.5	-	-	-	Handling	GEO
	COR2	0.5	-	-	-	Handling	GEO
Triton TOR	TOR3C	1.1	330	14.5	11.7	Gage Area	Control
	TOR4C	1.1	190	5.6	3.3	Grip Edge	Control
	TOR5C	1.1	370	9.6	3.0	Grip Edge	Control
	TOR1	1.1	130	1.2	0.9	Grip Edge	GEO
	TOR2	1.1	-	-	-	Handling	GEO
Triton TOR-RC	RC3C	1.8	240	6.0	2.9	Gage Area	Control
	RC1	1.8	180	4.7	2.7	Gage Area	GEO
	RC2	1.8	200	4.3	2.3	Grip Edge	GEO

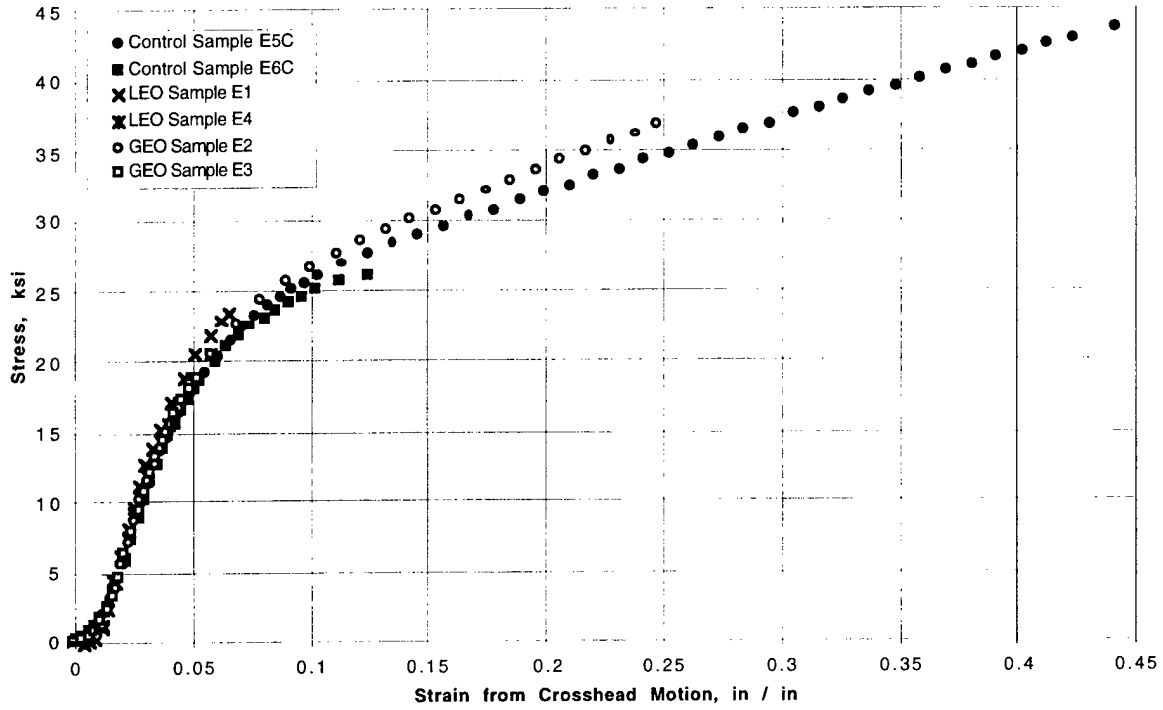

Figure 13A. Stress-strain curves for 0.0005 inch uncoated Kapton E foil.

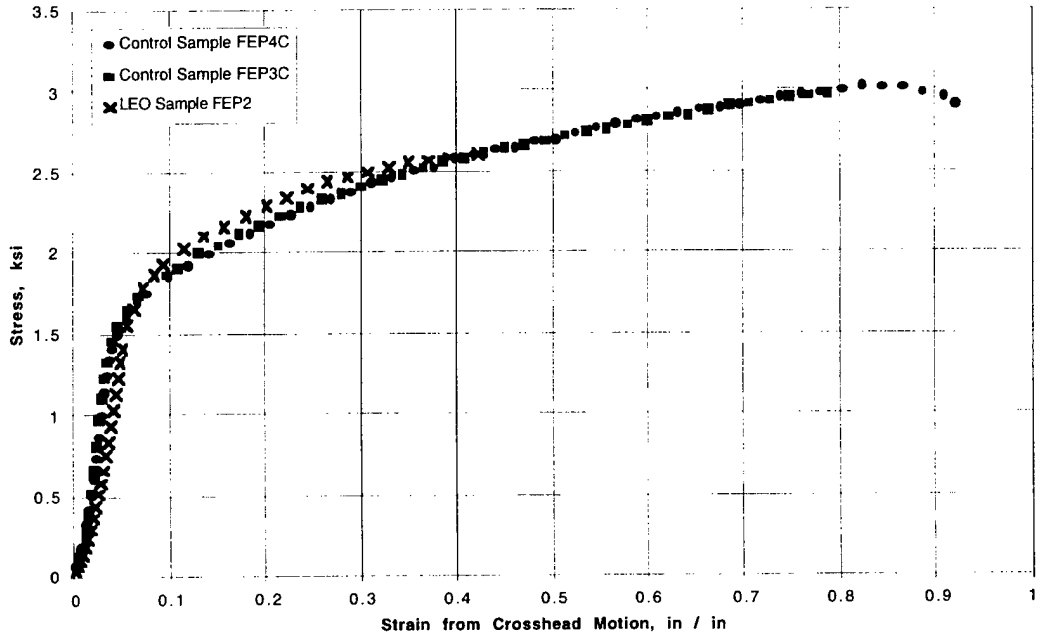

Figure 14A. Stress-strain curves for 0.0005 inch FEP Teflon foil.

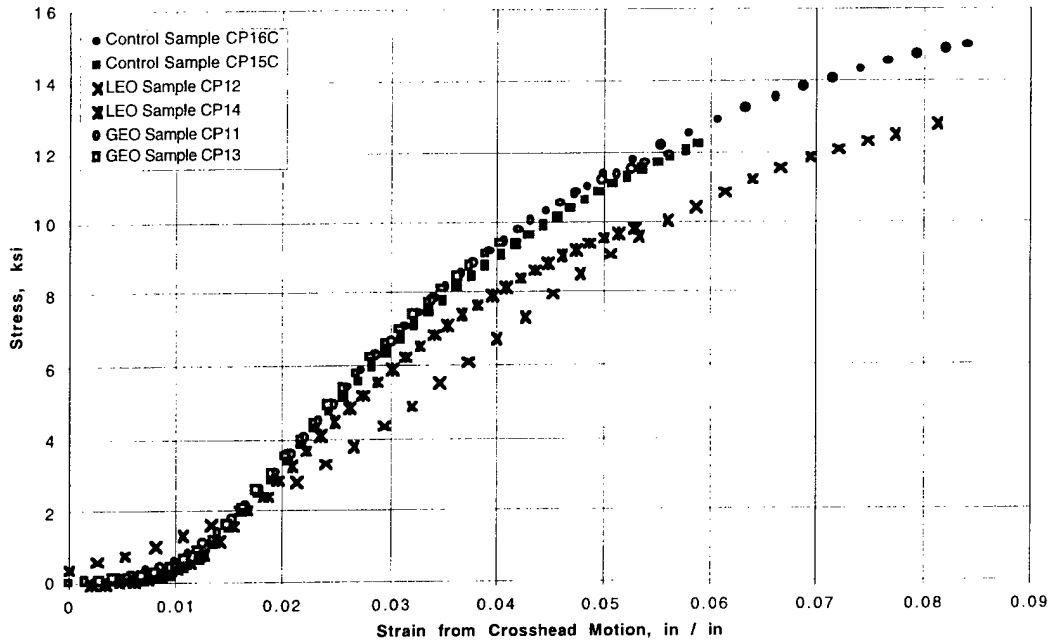

Figure 15A. Stress-strain curves for 0.0005 inch LaRC-CP1 foil.

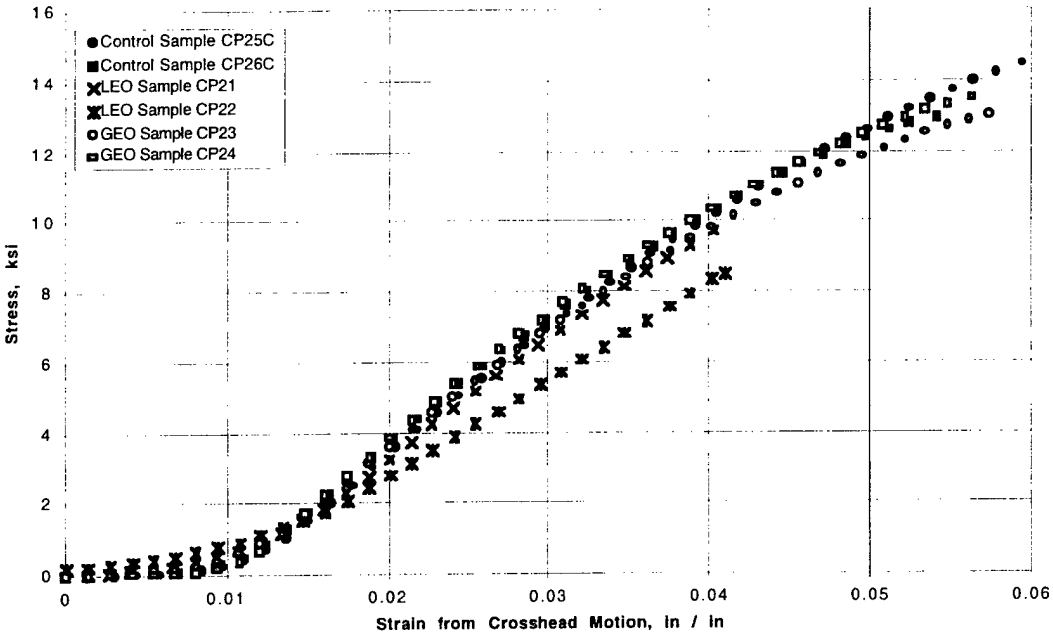

Figure 16A. Stress-strain curves for 0.0005 inch LaRC-CP2 foil.

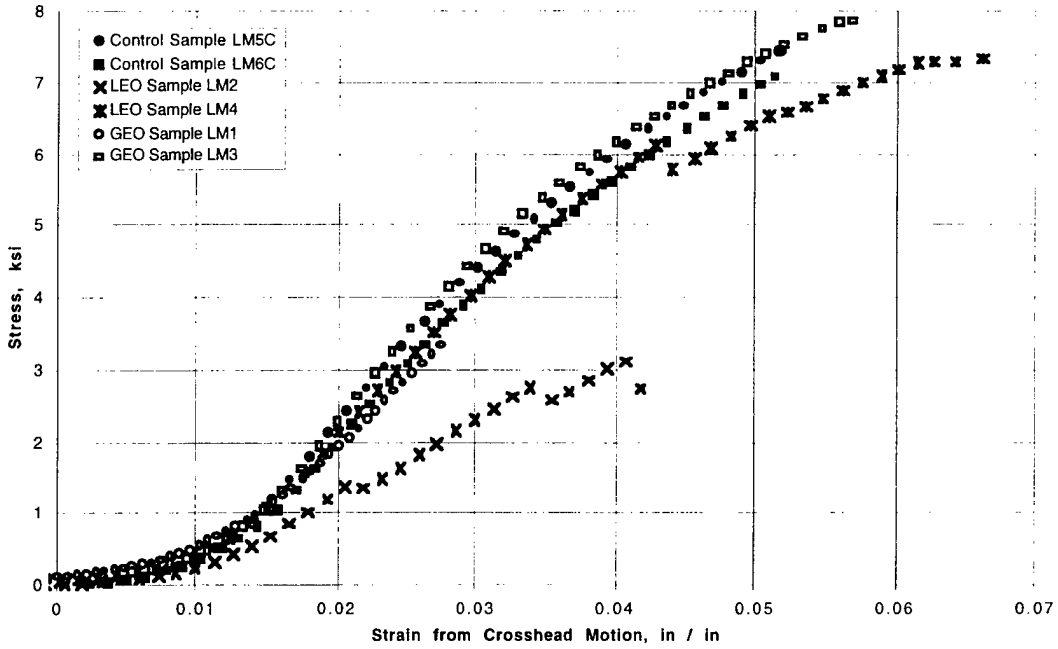

Figure 17A. Stress-strain curves for 0.0008 inch Triton TOR-LM foil.

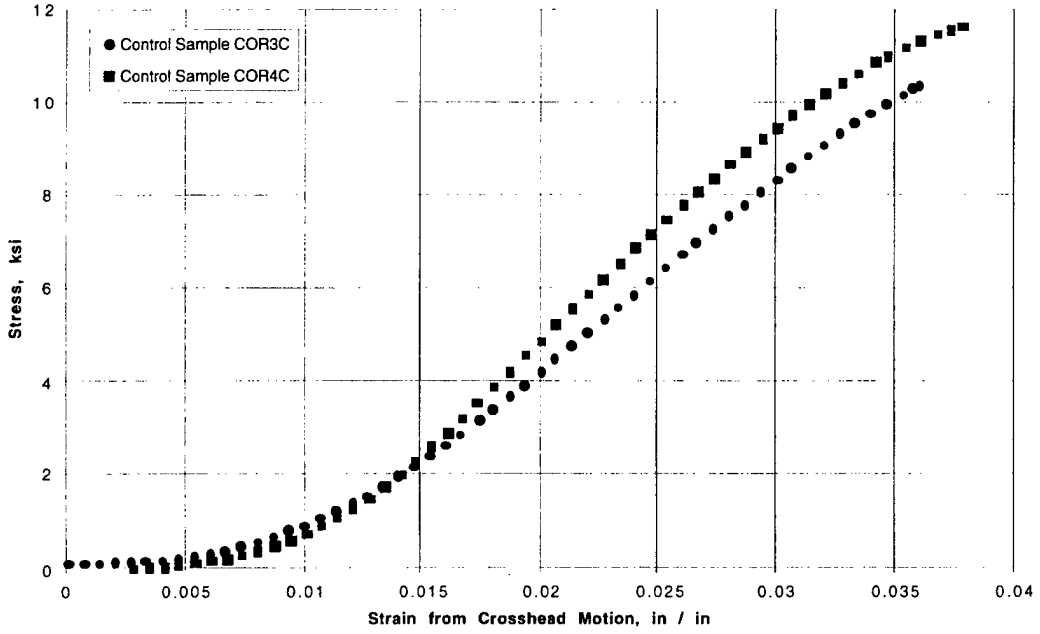

Figure 18A. Stress-strain curves for 0.0005 inch Triton Conductive COR foil.

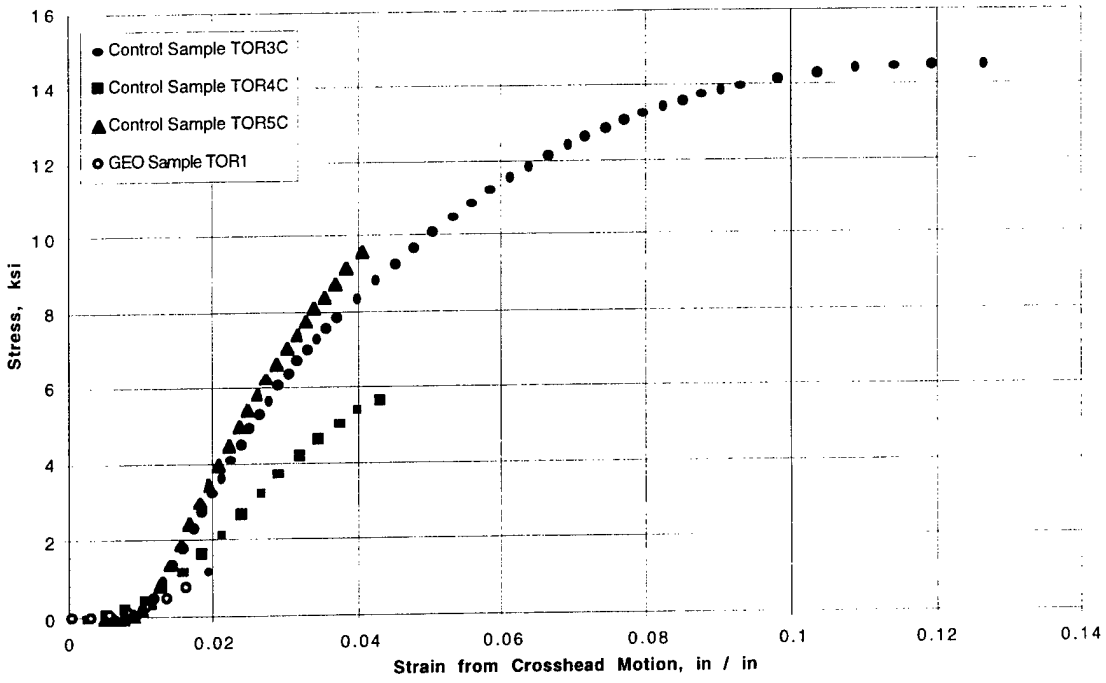

Figure 19A. Stress-strain curves for 0.0011 inch Triton TOR foil.

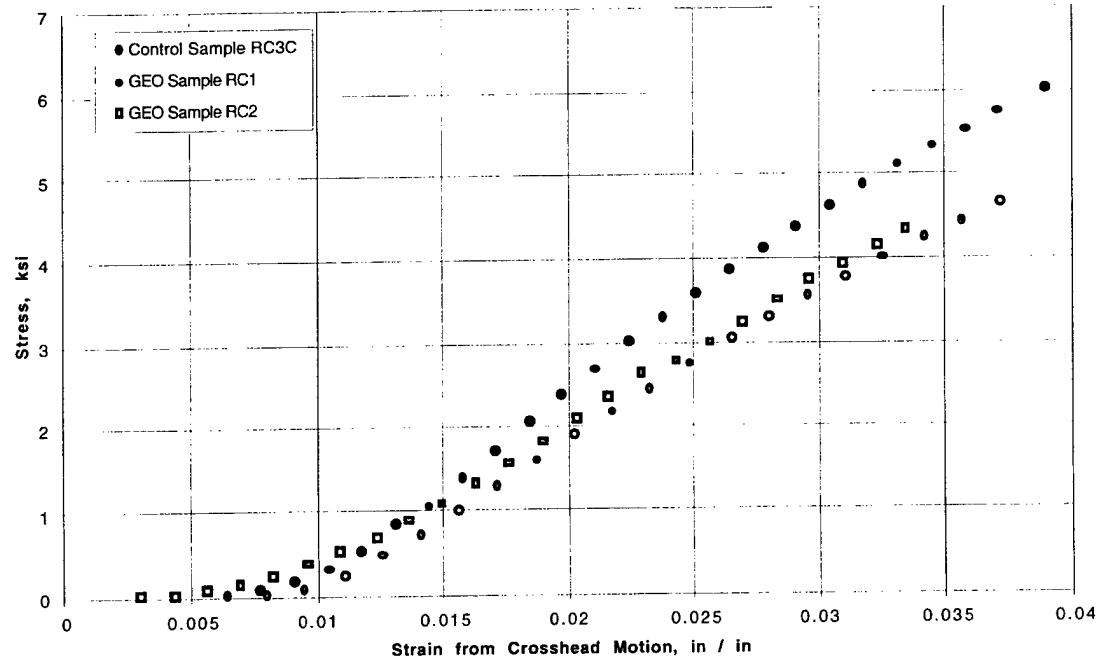

Figure 20A. Stress-strain curves for0.0018 inch Triton TOR-RC foil.

TECHNOLOGY OPERATIONS

The Aerospace Corporation functions as an "architect-engineer" for national security programs, specializing in advanced military space systems. The Corporation's Technology Operations supports the effective and timely development and operation of national security systems through scientific research and the application of advanced technology. Vital to the success of the Corporation is the technical staff's wide-ranging expertise and its ability to stay abreast of new technological developments and program support issues associated with rapidly evolving space systems. Contributing capabilities are provided by these individual Technology Centers:

Electronics Technology Center: Microelectronics, VLSI reliability, failure analysis, solid-state device physics, compound semiconductors, radiation effects, infrared and CCD detector devices, Micro-Electro-Mechanical Systems (MEMS), and data storage and display technologies; lasers and electro-optics, solid state laser design, micro-optics, optical communications, and fiber optic sensors; atomic frequency standards, applied laser spectroscopy, laser chemistry, atmospheric propagation and beam control, LIDAR/LADAR remote sensing; solar cell and array testing and evaluation, battery electrochemistry, battery testing and evaluation.

Mechanics and Materials Technology Center: Evaluation and characterization of new materials: metals, alloys, ceramics, polymers and composites; development and analysis of advanced materials processing and deposition techniques; nondestructive evaluation, component failure analysis and reliability; fracture mechanics and stress corrosion; analysis and evaluation of materials at cryogenic and elevated temperatures; launch vehicle fluid mechanics, heat transfer and flight dynamics; aerothermodynamics; chemical and electric propulsion; environmental chemistry; combustion processes; spacecraft structural mechanics, space environment effects on materials, hardening and vulnerability assessment; contamination, thermal and structural control; lubrication and surface phenomena; microengineering technology and microinstrument development.

Space and Environment Technology Center: Magnetospheric, auroral and cosmic ray physics, wave-particle interactions, magnetospheric plasma waves; atmospheric and ionospheric physics, density and composition of the upper atmosphere, remote sensing, hyperspectral imagery; solar physics, infrared astronomy, infrared signature analysis; effects of solar activity, magnetic storms and nuclear explosions on the earth's atmosphere, ionosphere and magnetosphere; effects of electromagnetic and particulate radiations on space systems; component testing, space instrumentation; environmental monitoring, trace detection; atmospheric chemical reactions, atmospheric optics, light scattering, state-specific chemical reactions and radiative signatures of missile plumes, and sensor out-of-field-of-view rejection.